Diagnosing Diabetic Retinopathy from Colored Fundus Images

Basmah Yakoub Anber

Submitted to the
Institute of Graduate Studies and Research
in partial fulfillment of the requirements for the degree of

Master of Science
in
Computer Engineering

Eastern Mediterranean University
September 2017
Gazimağusa, North Cyprus

Approval of the Institute of Graduate Studies and Research

Assoc. Prof. Dr. Ali Hakan Ulusoy
Acting Director

I certify that this thesis satisfies the requirements as a thesis for the degree of Master of Science in Computer Engineering.

Prof. Dr. Işık Aybay
Chair, Department of Computer Engineering

We certify that we have read this thesis and that in our opinion it is fully adequate in scope and quality as a thesis for the degree of Master of Science in Computer Engineering.

Assoc. Prof. Dr. Duygu Çelik Ertuğrul
Supervisor

Examining Committee

1. Assoc. Prof. Dr. Duygu Çelik Ertuğrul
2. Assoc. Prof. Dr. Önsen Toygar
3. Asst. Prof. Dr.Yıltan Bitirim

ABSTRACT

In this study, the problem of automatic detection of Diabetic Retinopathy (DR) has been addressed. As the technology advances, researchers are becoming more interested in intelligent medical diagnosis systems to assist screening for specific diseases such as diabetes and its complications. DR is a serious condition which can result in blindness if it is not diagnosed and controlled at early stage.

Medical experts diagnose DR from specific lesions in colored fundus images. There are different segments possibly appearing in fundus images including Optical Disk (OD), Blood Vessels (BV), Dark Lesions (i.e. Microaneurysm (MA) or briefly Aneurysm, Hemorrhage (H) and Neuvascularization (NV)), and Light Lesions (i.e. Hard Exudates (HE) and Cotton Wool Spots (CVS)). In this thesis, an automated system is proposed for automatic detection of lesions and accordingly grading DR. The proposed system is implemented as follows: After removing noisy area, optical disk is discovered in images based on a histogram template method. Then, using thresholding a black and white mask is produced to remove optical disk from fundus images. The network of blood vessels should also be removed. Based on Kirsch edge enhancement technique, blood vessels are masked. The next step of segmentation is searching for dark and light lesions. In the next phase, six features related to anatomical characteristics of anomalies in retinal images are extracted. These features are related to size, shape, color and brightness of the regions. Support Vector Machine (SVM) classifier is the last stage of the system. Light lesions and dark lesions are separately classified into their corresponding anomalies using linear SVM classifier. 5-fold cross validation is used to avoid bias in selection of train and test sets. Experimental results

conducted on four data sets including DIARETDB0, DIARETDB1, STARE and HRF have proved that accuracy, sensitivity and specificity of the proposed system are comparable or superior to state-of-the-art methods. In the last step, based on the detected abnormal lesions, the degree of severity of DR is automatically defined.

Keywords: Diabetic Retinopathy, Automatic Detection, Fundus Image, Abnormal Lesions, Image Segmentation, Feature Extraction, Classification.

ÖZ

Bu çalışmada, Diyabetik Retinopati'nin (DR) otomatik olarak saptanması sorunu ele alınmıştır. Teknoloji ilerledikçe, araştırmacılar diyabet gibi komplikasyonları belirli hastalıklar için medikal taramada yardımcı olmak için akıllı teşhis sistemleri üzerinde daha fazla odaklanmışlardır. DR ciddi bir durumdur, erken teşhis edilip kontrol edilmediğinde körlüğe neden olabilir.

Tıbbi uzmanlar, renkli göz dibi (fundus) görüntülerinde spesifik lezyonlardan DR'yi teşhis edebilmektedirler. Optik Disk, Kan Damarları, Karanlık Lezyonlar (örneğin, Mikroanevrizma veya kısaca Anevrizma, Kanama ve Neuvaskülarizasyon) ve Işık Lezyonlar (örneğin, Sert Yırtıklar ve Pamuk Yünü Noktaları) dâhil olmak üzere fundus görüntülerinde olası farklı bölümler görülebilmektedir. Bu tez çalışmasında, lezyonların otomatik olarak saptanması ve buna göre DR'nin derecelendirilmesi için otomatik bir sistem önerilmiştir. Önerilen sistem şu şekilde uygulanmıştır: alan kaldırdıktan sonra, histogram şablon yöntemine bağlı olarak görüntülerde optik disk bulunur. Ardından, eşik değerleme ile siyah beyaz bir maske üretilerek, optik diski fundus görüntülerinden çıkarılması yapılır. Kan damarları ağı da kaldırılması gerekmektedir. Kirsch kenar iyileştirme tekniğine göre, kan damarları da maskelenmiştir. Bölümlemenin sonraki basamağı karanlık ve hafif lezyonları araştırmaktır. Bir sonraki aşamada, retina görüntülerde anomalilerin anatomik özelliklerine ilişkin altı öznitelikleri çıkarılmıştır. Bu öznitelikler bölgelerin büyüklüğü, şekli, rengi ve parlaklığı ile ilgilidir. Destek Vektör Makinesi (SVM) sınıflandırıcı, sistemin son asamasıdır. Işık lezyonlar ve karanlık lezyonlar ayrı doğrusal SVM sınıflandırıcı kullanarak bunlara karşılık gelen anomaliler ayrılır.

Eğitim ve test setlerinin seçiminde sapmayı önlemek için 5 kat çapraz doğrulama tekniği kullanılır. DIARETDB0, DIARETDB1, STARE, ve HRF veri setleri üzerinde yapılan deneysel sonuçlar, önerilen sistemin doğruluğunun, duyarlılığının ve özgünlük, güncel yöntemlerle kıyaslanabilir veya daha iyi sonuçlar ürettiğini kanıtlamıştır. Diğer çalışmalarda kulanılan renkli göz dibi görüntü sayıları ile kıyaslandığında, bu çalışmamızda toplam 289 renkli göz dibi (fundus) görüntüleri seçilmiş ve değerlendirilmiştir. Bu doğrultuda, sistemin genel performansı kabul görecek nitelikte sonuçlar üretmiş. Son aşamada, tespit edilen anormal lezyonlara dayanılarak, DR şiddeti otomatik olarak zemin gerçeklere göre kıyaslanmıştır.

Anahtar Kelimeler: Diyabetik Retinopati, Otomatik Algılama, Fundus Görüntüsü, Anormal Lezyonlar, Görüntü Parçalama, Öznitelik Çıkarma, Sınıflama.

DEDICATION

In memory of my father Yakoub Anber.

To my mother Ana'am Ahel.

To my brothers Samir, Mounir, Mohamed and Mahdi.

To Ebtesaam my sister and her daughter Rama.

Last but not least to all my new great friends that I met here in EMU, especially Dr. Anas and his wife Nagham who were my family to me in Famagusta.

ACKNOWLEDGMENT

I would like to thank God for everything he offered to me. Special thanks to my supervisor Asst. Prof. Dr. Duygu Çelik Ertuğrul for her amazing support, notes and advices that leaded me in writing my thesis.

Thanks to my mom's prayers, and to my family support. Thanks to every single person supported me a penny for my education.

To Mahdi my brother who supported me morally and financially to reach this point.

Thanks to my close friends Zena, Nagham, Batoul, Mariam, Ghazaal, Soran and my friend Amira in Palestine for being always beside me.

Thanks to my nieces and nephews who wished success me in this step of my life. I love you all.

TABLE OF CONTENTS

LIST OF TABLES

LIST OF FIGURES

LIST OF ABBREVIATIONS

ANN	Artificial Neural Network
BPN	Back Propagation Neural Network
CWS	Cotton Wool Spots
DR	Diabetic Retinopathy
DT	Decision Tree
GA_CFS	Genetic Algorithm with Correlation based Feature Selection
GT	Groundtruth
H	Hemorrhage
HE	Hard Exudates
KNN	k Nearest Neighbor
LSR	Least Square Regression
MA	Microaneurysm
MLP	Multilayer Perceptron
NPDR	Non-proliferative Diabetic Retinopathy
NV	Neuvascularization
OD	Optic Disk
PDR	Proliferative Diabetic Retinopathy
ROI	Region of Interest
SE	Soft Exudates
SED	Sobel Edge Detector
SVM	Support Vector Machines

Chapter 1

INTRODUCTION

Diabetic Retinopathy (DR) is an eye disease, which damages Blood Vessels (BVs) in the retina because of high blood sugar levels [1]. Damaged BVs can swell and leak or stop passing blood through. There are two main stages of DR: Non-proliferative Diabetic Retinopathy (NPDR) and Proliferative Diabetic Retinopathy (PDR). NPDR is the early stage of diabetic eye disease that can be classified into three degrees of severity; as mild, moderate, and severe based on the presence or absence of retinal bleeding [2, 3]. PDR is the advanced stage of diabetic eye disease and it happens when small blood vessels grow from the surface of the retina [2, 3]. This is called neovascularization (NV) [2]. In [3], DR grading defined by American Academy of Ophthalmology is represented which is called "International Clinical Diabetic Retinopathy Disease Severity Scale". These scales are shown on Table 1.

Blindness is the leading cause of DR. However, early detection and prompt treatment of the disease can prevent visual loss of more than 90% of patients [4]. Regularly screening of DR is an effective way to prevent blindness. An important screening approach in clinic is using fundus photography. The use of computer aided digital image processing has become popular in medicine to assist ophthalmologist in better diagnosis of DR.

Table 1: Diabetic retinopathy severity scale [3]

Grade	**Non-proliferative/Proliferative**	**Findings in Ophthalmoscopy Results**
Normal	None	No sign of abnormality
Mild	Non-proliferative Diabetic Retinopathy	Signs of MA only
Moderate	Non-proliferative Diabetic Retinopathy	Including more abnormalities than just MA such as H and/or HE and/or CWS but not all of them
Severe	Non-proliferative Diabetic Retinopathy	Including any of the following findings: — More than 20 H lesions in each of the four quadrants of retina — Definite MA in at least two quadrants — Prominent intra-retinal microvascular abnormalities in at least one of the quadrants (such as H and MA together)
Proliferative diabetic retinopathy (PDR)	Proliferative Diabetic Retinopathy	At least one of the following anomalies: — Neuvascularization — Vitreous/pre-retinal bleeding (H, MA, HE, CWS in all quadrants)

Abnormally high blood sugar level results in weakening of the retinal capillaries. This causes small swelling in the side of a BVs in retina known as Microaneurysms (MAs) [4]. MAs appear as small, red dots in the superficial retinal layers. *Mild NPDR* can be indicated by the presence of at least one MA. Rupture of MAs in the deeper layers of the retina, forms Hemorrhages (Hs). Since their appearance is like a dot, they are called "dot-and-blot" Hemorrhages [4]. Breakdown of the blood-retina barrier causes leakage of proteins, lipids, and protein from the vessels which is called Hard Exudates (HE) [3, 4]. *Moderate NPDR* includes the presence of multiple MA, dot-and-blot Hs and HEs. As NPDR progresses, eventually the affected vessels get obstructed. Obstructed vessels may cause infarction of the nerve fiber layer resulting in fluffy, white patches called Cotton Wool Spots (CWS) which also known as Soft Exudates (SE) [3, 4].

Severe NPDR can be characterized by CWS and intra-retinal microvascular abnormalities [2].

People who have had diabetes for 20 years or more are more likely to have DR [5]. DR causes serious visual consequences. One of the leading causes of DR is blindness [6]. Therefore, early detection and diagnosis of this disease is significantly important in controlling the progress of the disease. Detection of DR is done through regular screening. Regular screening employs health service resources which is time consuming and brings significant amounts of cost when it comes to a large number of people.

Image processing techniques can be used as computer aided systems to automate the process of detection of DR in order to reduce the workload associated to manual screening as well as save diagnosis costs and time. Image processing uses images of retinal vessels to classify normal and abnormal images of retina. Digital fundus cameras are used for acquiring retinal images. Figure 1 [7] shows fundus photographs of normal retina and diabetic retinopathy.

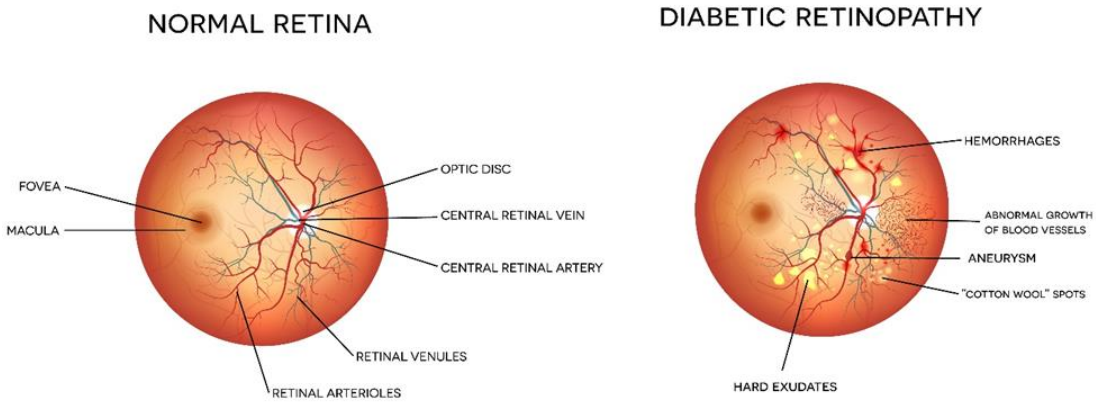

Figure 1: Fundus photographs of normal retina and diabetic retinopathy [7]

In Figure 2 [8], PDR versus NPDR is illustrated and it can be seen that in PDR level, BVs are grown abnormally.

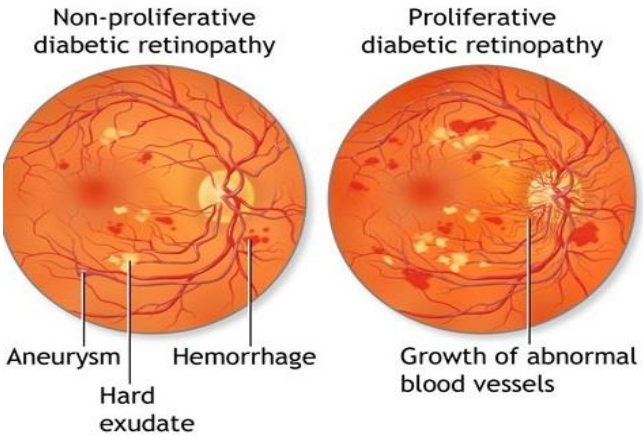

Figure 2: Non-proliferative DR versus proliferative DR [8]

BVs, fovea and Optic Disc (OD) are some of eye features which can be used for automatic classification of DR. Any change in the shape, color, or depth of these features can provide useful information about DR [9]. These features are extracted from diabetic retinal pictures in automatic detection of DR. OD is extracted in case of exudates detection. The fovea and BVs are extracted in case of MAs, Hs and Neovascularization (NV) [9]. DR indicative lesions include dark and bright lesions. MAs and Hs are classified as dark lesions. Exudates are classified as bright lesions [9]. So, automatic detection of distinct lesions is an important step in development of DR automatic detection systems. In this study, automatic detection of DR based on fundus images is addressed. In addition, a rule-based system is defined to assign a severity scale to each image according to detected anomalies.

The remaining of this dissertation is organized as follows. The second chapter indicates the recent studies about automatic segmentation of retinal images and DR.

The third chapter explains the system architecture. In chapter four, methodology of the study is described. Chapter five reports experimental results on DIARETDB0 [10], DIARETDB1 [11], STARE [12] and HRF [13] data sets. Finally, in the last chapter, experimental results are discussed and the study is concluded.

Chapter 2

LITERATURE REVIEW

2.1 Automatic Detection of DR

As digital image processing techniques developed, the use of computer aided fundus image processing become popular in clinical work in order to help ophthalmologist in better diagnosis of DR [14-17]. OD and BVs are normal features of fundus image [14]. Exudates and Hemorrhages are main abnormal features of DR [14]. The detection of these features is needed for diagnosing of DR. Different algorithms have been proposed in the literature for segmentation of different features in retinal images [9, 17]. The features extracted from fundus images are then to be processed in higher levels for detection of retinopathy with degree of severity.

One of the main problems of automatic diagnosis of DR from fundus images is the lack of common evaluation method [14]. Second problem is that finding a verified GT image database for evaluation of various proposed diagnosis algorithms and comparison of different algorithms in detection of DR [10, 11, 14]. Most of the proposed diagnosis algorithms are used shape, color, and area of DR findings [9-13]. This kind of detection is known as direct detection. On the other hand, the detection of DR can be done indirectly by comparing fundus images of a patient's eye in different time intervals [14]. Both approaches consider abnormal features in fundus images caused by DR. These abnormalities are shown in Figure 3 [14].

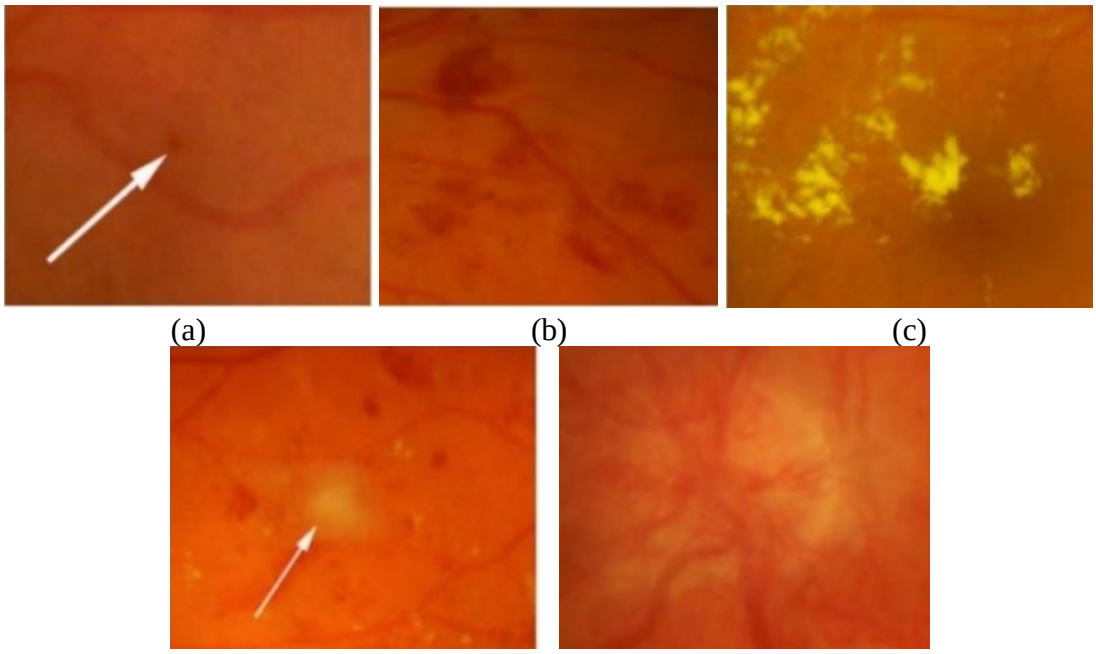

Figure 3: Different abnormalities in DIARETDB0 [14]
(a) MA (b) H (c) HE (d) SE (e) Neovascularization

It has been mentioned in [14] that a tool is necessary to detect anomalies and compare current proposed methods for getting more reliable results. Therefore, a verified GT file and an identical evaluation method are needed to make automatic diagnosis of DR more reliable and practical. For these reasons, a verified GT image database and an evaluation protocol are discussed in [18]. The database which is called DIARETDB0 [10] includes a set of verified images related to DR with their medical information and it is publicly available for all researches.

In addition to DIARETDB0, another data set from the same institute has also been collected and published. This fundus data set named DIARETDB1 [11]. This is a public database for benchmarking diabetic retinopathy detection from digital images. The main objective of the design has been to unambiguously define a database and a testing protocol which can be used to benchmark diabetic retinopathy detection

methods. By using this database and the defined testing protocol, the results between different methods can be compared. For groundtruth (GT) preparation Independent markings from 4 medical experts were collected by using a software tool provided for image annotation. The computer displays used in the collection process were not calibrated. A person with medical education and solid experience in ophthalmology was considered as an expert [11].

Another commonly used colored fundus image data set is high-resolution fundus or HRF data set [13]. This database has been established by a collaborative research group to support comparative studies on automatic segmentation algorithms on retinal fundus images. The public database contains at the moment 15 images of healthy patients, 15 images of patients with diabetic retinopathy and 15 images of glaucomatous patients. Binary gold standard vessel segmentation images are available for each image. Also the masks determining field of view (FOV) are provided for particular datasets [13]. The gold standard data is generated by a group of experts working in the field of retinal image analysis and clinicians from the cooperated ophthalmology clinics.

The STARE (STructured Analysis of the Retina) project is also one of the famous resources of fundus images [12]. The STARE Project was conceived and initiated in 1975 by Michael Goldbaum, M.D., at the University of California, San Diego. It was funded by the U.S. National Institutes of Health. During its history, over thirty people contributed to the project, with backgrounds ranging from medicine to science to engineering. Images and clinical data were provided by the Shiley Eye Center at the University of California, San Diego, and by the Veterans Administration Medical

Center in San Diego. The full data set comprises of almost 400 images and a GT of detected disease. The GT file contains list of diagnosis codes and diagnoses for each image. A total of 44 possible manifestations were queried to the experts during data collection and then reduced to 39 values during encoding. Diagnoses codes are for different illnesses including DR [12].

According to a published technical report in related with DIARETDB0 image data set [10], some common steps are followed in most diagnosis algorithms to find abnormalities in fundus images. These common steps are as follows: At first, image enhancement is done. In image enhancement, different methods are applied such as median filtering, local contrast enhancement, histogram specification, iterative robust homographic surface fitting, etc. Secondly, candidate DR features are detected. Thirdly, images are classified into a correct DR category [9, 17].

The proposed evaluation protocol in [14] uses *Sensitivity* and *Specificity* to evaluate diagnosis algorithms. It works as follows: at first, sensitivity and specificity of the manually segmented images by human observer are calculated and stored in a file. This file considered as Ground Truth (GT) file. Then, the sensitivity and specificity of the image using diagnosis algorithm is calculated. At the end, the calculated results using diagnosis algorithm is compared with the results which are stored in GT file. The proposed database and evaluation method have some drawbacks which are needed to be addressed in further studies.

2.2 Optical Disk (OD) Detection

One of the first challenges in the procedure of DR detection is removing OD. This round shaped light area is required to be located and masked from the images using image processing techniques. In [9], the algorithms that are used to detect the OD are Sobel Edge Detector (SED) [15] and Least Square Regression (LSR) [16]. SED is a well-known edge detection technique in image processing [15]. In [9], SED is applied to get the contour of the OD of the candidate area. Estimated circle of the OD mask is obtained based on the result of SED using LSR. A sample detected the OD is shown in Figure 2 4 [9].

Figure 4: A sample detected optical disk [9]

The method firstly finds the brightest pixel in the image and then sets it as the location of the OD. In other words, OD is assumed as a completely circular shaped segment with its center located on that pixel. This method finds an approximate coarse mask for OD as shown in Figure 5 and also in [17]. This method is not accurate and precise although it is computationally efficient.

Akram, U. [18], another method is proposed for OD localization and detection based on Hough Transform [19]. Firstly, fundus image is converted into gray scale image. Secondly, an averaging filter is applied to it remove noise and lesion artifacts. As a third step, the location of OD is detected based on the histogram of gray level image as the area containing OD has relatively larger gray levels. In fourth step, the location of OD helps to extract the boundaries using Hogh transform. Hough tranform is based on mathematical formula which defines the shape of a region of interest. For OD detection, this is defined as a circle based on the formula defined in [20]. An example image in which OD localization and segmentation have been applied is shown in Figure 6 [20].

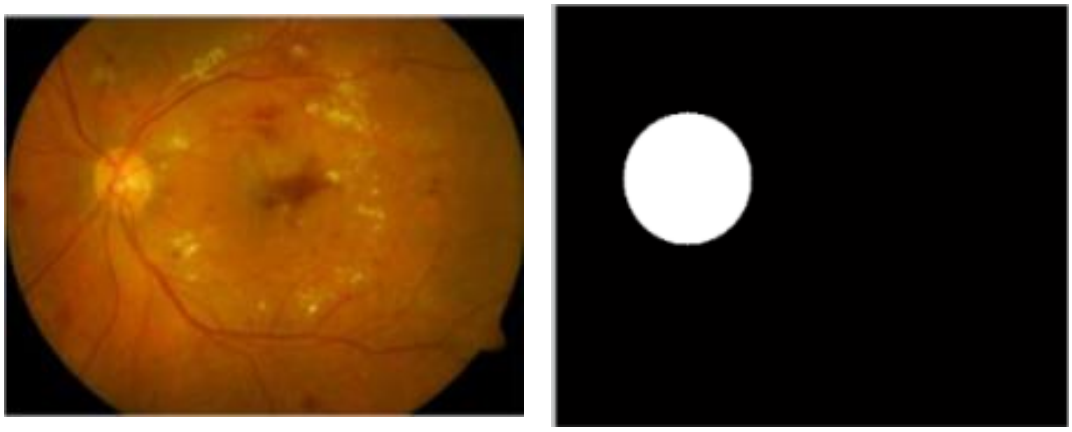

(a) (b)

Figure 5: A sample optical disk mask [17]
(a) Resized Image
(b) Mask

Argade et al. [21] applied SED and Ellipse Fitting for detection of OD and optic cup. They applied a preprocessing stage including resizing retinal gray images by converting the RGB images into gray scale images. As a next, they applied median filtering to reduce distortions in image and suppress the noise without blurring sharp

edges. Then, OD, Optic Cup, Exudates and BVs are detected [21]. SED and Ellipse Fitting [16] are used for detection of OD and Optic Cup as shown in Figure 7.

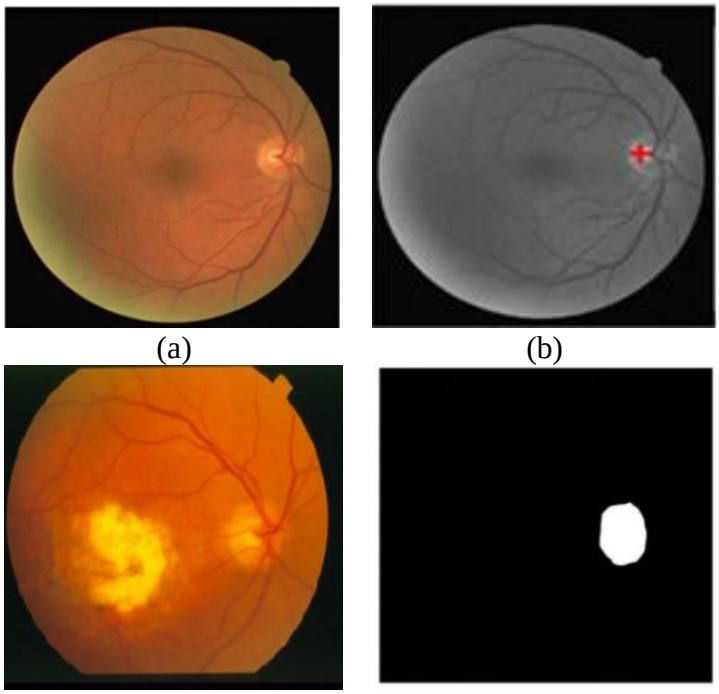

(a) (b)

(c) (d)

Figure 6: OD Localization and Detection [20]
(A) Original Retinal Image
(B) Localized OD
(C) Original Retinal Image
(D) Segmented OD

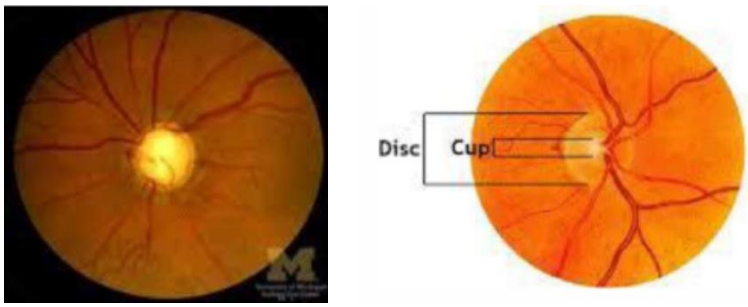

(a) (b)

Figure 7: Cup and OD detection [16]
(A) Original Image
(B) Optic Disc (OD) and Cup

OD appears as a bright yellowish and elliptical object in a healthy retinal image. Wankhede [22], applied a template-based method for OD detection has been proposed. OD shares some properties with bright lesions such as pixel intensity and color. Hence, information of OD in DR diagnosis algorithms should be avoided. Also, location of OD is important in localization of the fovea and detection of other abnormalities related to OD. As a result, OD segmentation has an important role in automatic diagnosis of DR.

Therefore, several different methods are suggested in literature for the detection of OD. These methods are classified into two groups [22]. First group is based on shape, color and structure of OD, and second group is based on the retinal vasculature for locating the OD. The algorithm proposed in [22] for estimation of OD size and selection of OD region of interest (ROI) uses a predefined histogram template. Use of the histogram template of color planes is presented in [22]. Median filter and adaptive contrast enhancement is applied on retinal images to remove intensity variations. A rectangular ROI, based on the location of OD is cropped. Then histogram of red plane, green plane and blue plane of ROI is calculated and stored as a template.

Figure 8 displays histograms of color planes of OD ROI and it is found out that different retinal images has almost same color histogram of OD ROI [22]. Therefore, template matching can be used for OD detection. Their proposed method is tested on DRIVE database [22] containing 40 retinal images. The results have been shown that the proposed algorithm achieves acceptable success rate in OD detection. Performance and time required for detection of OD of their proposed algorithm are compared with

other researcher methods and the retrieved results have been shown that their proposed algorithm outperforms all other methods in terms of performance and time [22].

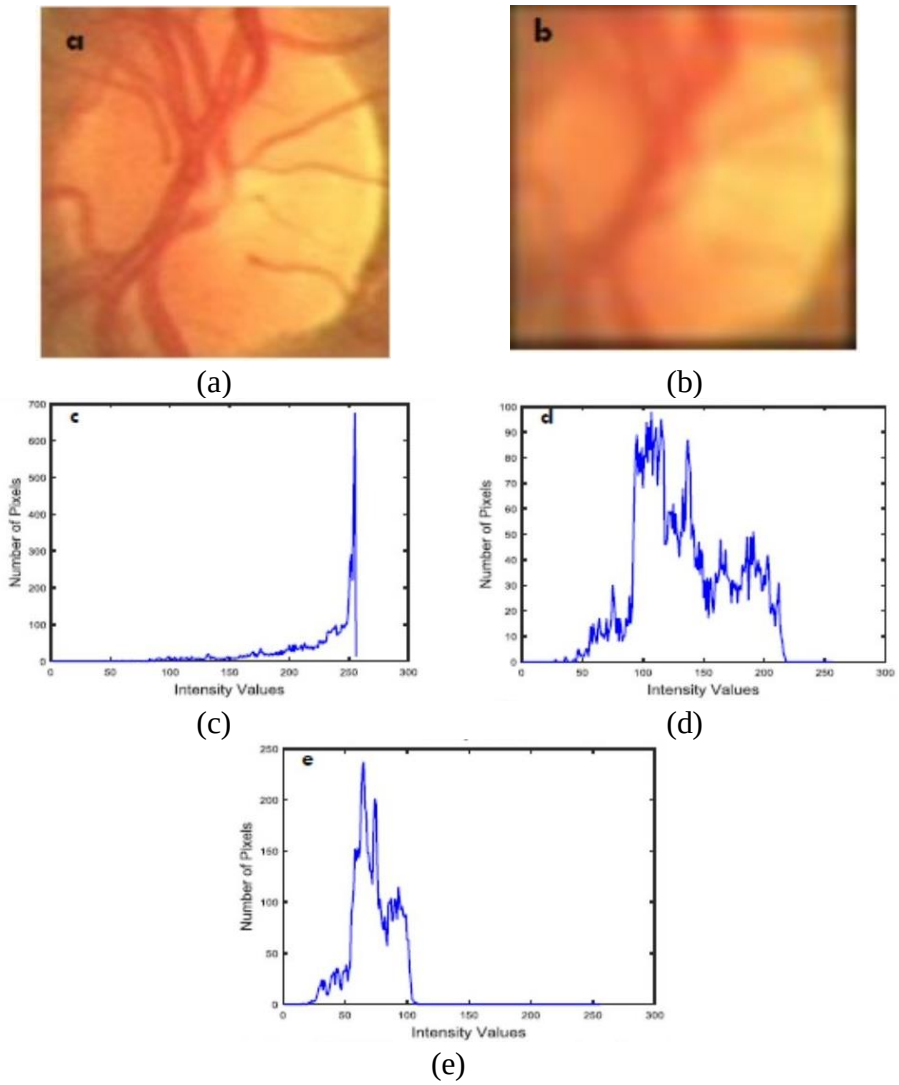

Figure 8: Template based histogram matching [22]
(a) ROI containing OD candidate
(b) Result of median filtering
(c) Histogram of red plane
(d) Histogram of green plane
(e) Histogram of blue plane

2.3 Segmentation of Blood Vessels (BVs)

The information about BVs, such as length, width, diameter and branching pattern provide useful information for diagnosis of DR. Therefore, extraction of BVs from fundus images is important for DR detection. A method which uses the Kirsch's templates [23] is proposed by Bhadauria et al. in [24] to extract BVs from fundus images. The proposed method consists four steps. The first step is applied edge detection of BVs in which Kirsch template is used. Kirsch convolution kernels are 3x3 filters to enhance edges in 8 different angles starting from 0 to 315. These kernels of Kirsch are shown in Figure 9.

$$\begin{bmatrix}-3 & -3 & 5\\ -3 & 0 & 5\\ -3 & -3 & 5\end{bmatrix}\begin{bmatrix}-3 & 5 & 5\\ -3 & 0 & 5\\ -3 & -3 & -3\end{bmatrix}\begin{bmatrix}5 & 5 & 5\\ -3 & 0 & -3\\ 3 & -3 & -3\end{bmatrix}\begin{bmatrix}5 & 5 & -3\\ 5 & 0 & -3\\ -3 & -3 & -3\end{bmatrix}$$

$$\begin{bmatrix}5 & -3 & -3\\ 5 & 0 & -3\\ 5 & -3 & -3\end{bmatrix}\begin{bmatrix}-3 & -3 & -3\\ 5 & 0 & -3\\ 5 & 5 & -3\end{bmatrix}\begin{bmatrix}-3 & -3 & -3\\ -3 & 0 & -3\\ 5 & 5 & 5\end{bmatrix}\begin{bmatrix}-3 & -3 & 5\\ -3 & 0 & 5\\ -3 & 5 & 5\end{bmatrix}$$

Figure 9: Convolution kernels of Kirsch [23]

False edge removal step is applied as a second step. In the third step, vessel junction restoration step is applied in order to restore broken vessel junctions by Kirsch template. In the last step, vessel labeling is applied in which the interior pixels of a vessel is filled. To evaluation of their proposed method, it is applied by the researchers on a dataset which consists 10 retinal images. Their results show that their method extracts BVs from retinal images successfully. Figure 10 displays BVs extraction from a retinal image [24].

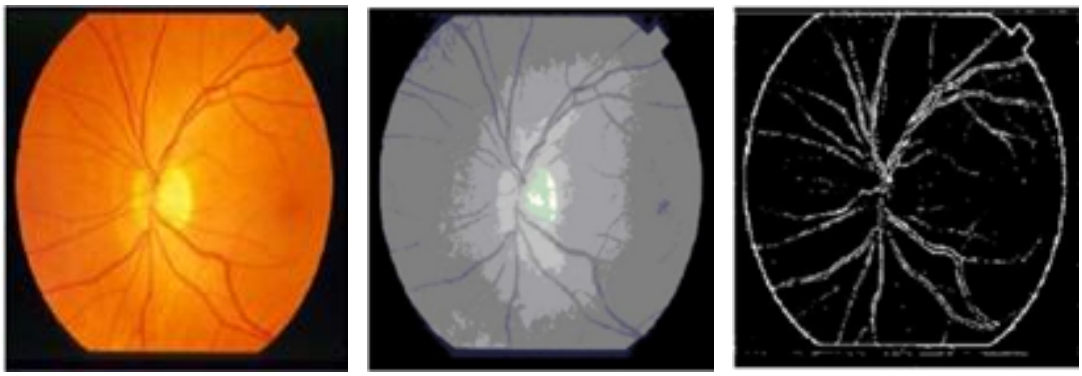

(a) (b) (c)

Figure 10: Blood vessel extraction [24]
(a) A sample Color retinal image
(b) Gray scale retinal image
(c) Extracted blood vessels from retinal image

First image shows the colored original image. Second image shows the converted colored image into grey scaled image. Third image displays processed grey scaled image by kirsch's templates which BVs extracted through edge detection technique [24].

Kirsch's method is also used by Li and Chutatape in [9] for detection of BVs and Exudates on the fundus image. The proposed system is validated on more than 30 fundus images. The retrieved results are shown to be promising in the detection of features [9].

In [18], Gabor filter is used for BVs detection. Since BVs are not completely visible in some images, BV enhancement step is applied to enhance the appearance of the low visibility BVs, especially thin vessels. For this purpose, 2-D Gabor wavelet is used according to its directional selectiviy abiliy. Finding a threshold value for this filtering method is a crucial issue. In [18], a hierarchical approach has been proposed in which

the threshold value is selected based on the histogram of the image. Figure 11 shows an example picture of segmented BVs [18].

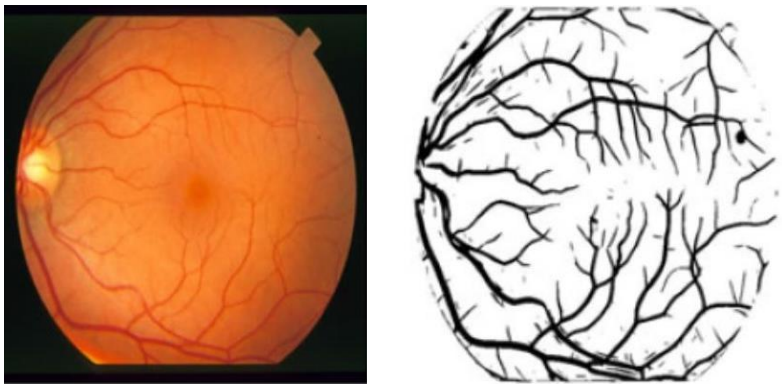

(a) (b)

Figure 11: Blood Vessel detection [18]
(a) Original retinal image (b) Segmented blood vessels

In [21], BVs are detected using Histogram Thresholding and Smoothing. Since BVs have a linear large and straight shape with gentle curves, the BVs have a specific histogram shape. Therefore, they can be detected by comparing histogram differences using a predefined threshold. Then, a smoothing algorithm is applied to remove noise and provides a fitter curve. Figure 12 shows an examination of the detected BVs by using this technique [21].

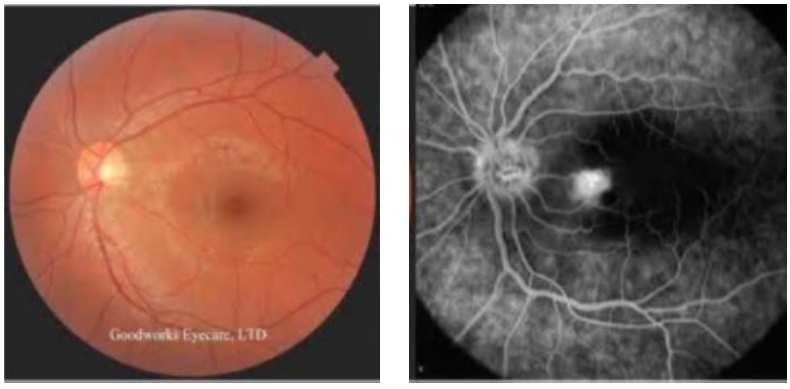

(a) (b)

Figure 12: Detection of blood vessels [21]
(a) Original image (b) Extracted blood vessels

2.4 Lesions and Feature Extraction

MAs, Hs, HEs and CWS (also known as SEs) are the most distinctive sings of DR. MAs and Hs are known as dark lesions. The HEs and SEs are known as bright lesions. Detection of dark and bright lesions are important for early detection of DR. Digital Diabetic Retinopathy System (DDRS) is proposed in [18] as a computer aided system for early detection of DR. The proposed method consists of three steps in order to detect DR. The complete flow chart of proposed DDRS is shown in Figure 13.

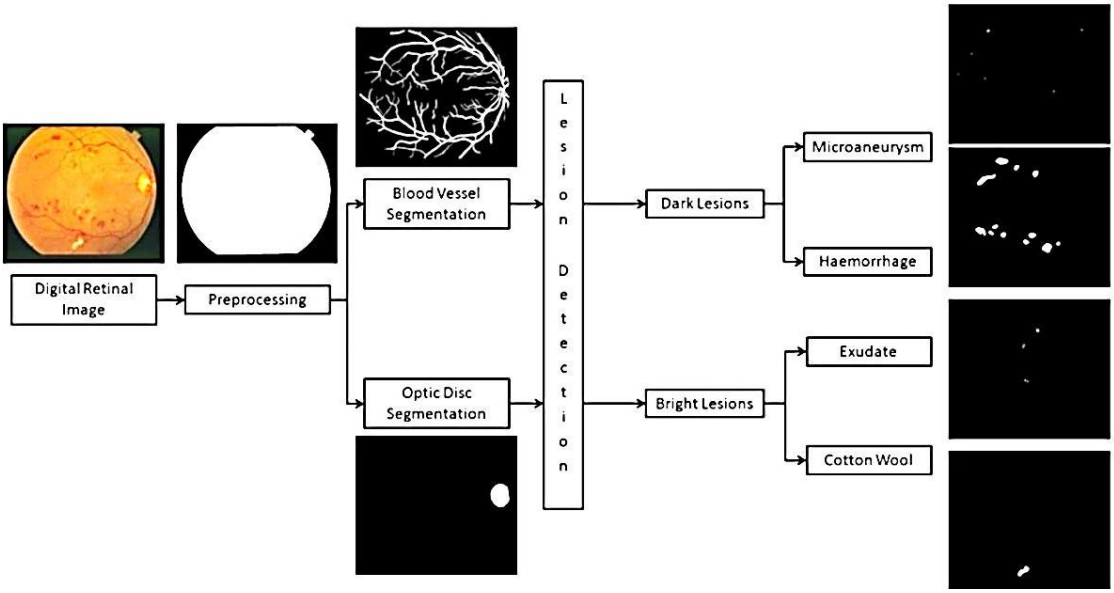

Figure 13: Flowchart of DDRS discussed in [18]

Light and dark lesions are segmented by using a thresholding approach after removing noise and masking OD and BVs from original fundus image. For each region, 6 features are extracted including ***area, mean hue, mean saturation, mean value, eccentricity***, and ***mean gradient*** magnitude. These features are extracted according to the characteristics of lesions listed in Table 2.

Table 2: Classification features of DR regions, Cataract, and Drusen diseases [18]

Lesions	Color	Size	Shape	Edge	Class
MICROANEURYSM (MA)	Dark red	Small	Round	Clear	Dark
HEMORRHAGE (H)	Dark red	Small-large	Dot-flame shaped	Clear-blur	Dark
HARD EXUDATE (HE)	Yellowish	Small-large	Irregular	Sharp	Bright
COTTON WOOL SPOT (CWS)	Whitish	Small-medium	Oval shaped	Blur	Bright
CATARACT	Blunted color	Various sizes	A circular-shaped	Cloudy	Bright
DRUSEN	Yellow or off-white	Various sizes	Wavy lines	Not clear	ND

As stated in Chapter 1, one of the primary signs of DR and main causes of blindness are *Exudates*. Therefore, early detection of exudates is very vital for patients. This is the main aim of an study by Gowda et al [25].

Hue, intensity of the image, standard deviation of intensity, distance between mean of OD pixels and pixels of exudates and non-exudates and mean intensity features are considered as inputs of the classifier. Artificial neural network (ANN) classifier is used to detect the presence or absence of exudates in the retinal images [25].

Before feeding features to classifier, a feature selection method is applied to find the best features for classification of exudates. Training and testing of classification methods is difficult if too many features used in training and testing the classifiers. As a result, selecting a subset of features to eliminate irrelevant and redundant data have a great importance for classification methods. Decision Tree (DT) and gGenetic Algorithm with Correlation-based Feature Selection (GA_CFS) methods are used as feature selection methods. DT selects intensity, standard deviation of intensity and

distance between OD pixels and other pixels as relevant features and GA_CFS selects intensity, standard deviation of intensity, hue and distance between optic disk pixels as relevant features which they are considered as inputs to ANN classifier as well. The authors have claimed that experimental results are promising compared to other proposed methods [25].

2.5 Classification

Methods which are used for detection and classification are: Gaussian filter, k-nearest neighbor clustering, support vector machine, canny edge detection, fuzzy neural networks and many more. In [18], Fuzzy hybrid neural network classifier is proposed in the third step for detection of dark and bright lesions. The proposed classifier composed of two subnetworks, first one is fuzzy self-organizing layer and second one is multilayer perceptron (MLP). Detection of lesion pixels and grouping them into clusters is the task of fuzzy self-organizing layer. The outcome of this layer is clusters including dark and bright lesions. Classification of extracted candidates from first layer to the appropriate class is the task of MLP. The discussed DDRS (shown in Figure 12) is verified on 4 different retinal image databases which are DRIVE, STARE, DiaretDB0 and DiaretDB1. Accuracy and area under the ROC curve (AUC) is used as performance measurement tools. The results show that proposed method gives higher accuracy and AUC values in comparison with other recently published methods and outperforms all others [18].

As mentioned in prevoius section, feature selection and back propagation neural network (BPN) are used by Gowda et al. in [25] to see how it perform in detection of exudates. Our adopted method gives similar outputs as shown in Figure 4. Different experiments are conducted by considering three different sets of inputs for ANN. First

experiment considers all features as inputs, second one takes features selected by DT as inputs and third one consider features identified by GA_CFS method as inputs of ANN classifier. Sensitivity, Specificity, Recall, and Precision and F-measure are applied as performance measurement tools by [25]. As claimed in the paper, the performance of ANN classifier with inputs identified by both DT and GA_CFS is improved compared to the performance of ANN classifier when all features are used as inputs [25].

The method is proposed in [21] for automatic detection of DR is based on k Nearest Neighbor (kNN) classification. kNN classification algorithm is used for detection of exudates. Preprocessing include resizing retinal gray images, convert RGB images into gray scale images and at the end, median filter is used to reduce distortions in an image and suppresses noise without blurring sharp edges. Second step is feature relevance analysis. In this step, optic disc, optic cup, exudates and blood vessels are detected. After detecting OD and blood vessels as explained in previous sections, final step is classification using data mining. Decision tree is selected as classification method to decide whether an image belongs to normal retinopathy or diabetic retinopathy. Figure 14, displays complete architecture of proposed algorithm for detection of DR. The proposed method is tested and it is shown to be promising [21].

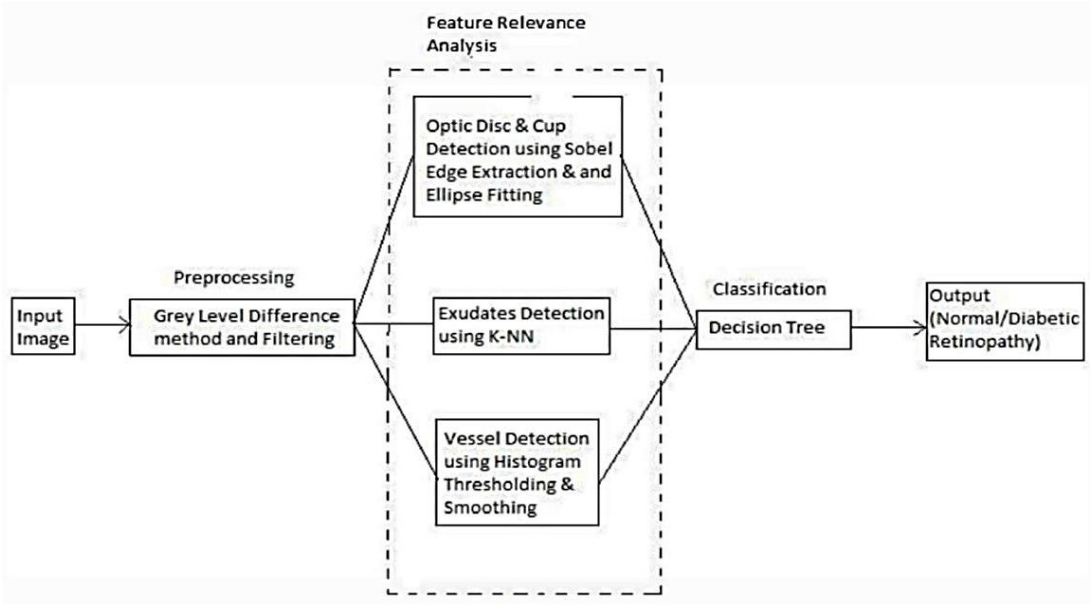

Figure 14: Flowchart of proposed system in [21]

In another study by Akram et. al [26], automated detection of exudates from colored fundus images has been addressed for DR detection. Exudates are important lesions for NPDR. In their study, they have utilized a filter bank approach to select candidate exudate regions in images. After preprocessing and contrast enhancement, candidate exudate regions are identified using Gabor filter bank. OD is then masked from the regions and 6 features are extracted from the remaining regions. Features include area, mean intensity, mean hue, mean gradient and two entropy-based measures. Classification is performed by Gaussian Mixture Models (GMM). Experimental results on 4 DR data sets comprising DIARETDB0, DIARETDB1, DRIVE and STARE have proved the efficiency of their proposed method [26].

Bourouis et al [27] have implemented a mobile application for retinal disease diagnosis. The intelligent mobile-based system proposed in [27], is an automated system for cataract and DR detection. Experiments have conducted on different retinal

image data sets. Performance of the system is claimed to be acceptable compared to medical expert diagnose.

Chapter 3

SYSTEM ARCHITECTURE

In this thesis, we have designed an automatic systems that detects diabetic retinopathy from colored retinal images. Since there are different parts appearing in fundus images, it is crucial to perform an accurate segmentation procedure as a first step. The segments which are to be seperated include *optic disk*, *blood vessels*, *dark lesions* and *light lesions*.

Initially, the *optic disk* and *blood vessels* segments should be masked from the retina images because they mislead the system when detecting lesions.

As the next step, *dark* and *light* lesions are segmented separately. From this stage on, there are two classifier approaches for detecting *light* and *dark anomalies*. Six features related to *size, shape, color,* and *intensity* are extracted from all detected segments. The SVM classifier approach is applied to distinguish between categories in *dark lesions* (*red small dots*, *H,* and *NV*). At the same time, another classifier is applied on *light lesions* to detect hard exudates from soft exudates. The architecture of the proposed algorithm is represented in Figure 15. In the following sections, each stage of this flowchart is explained in details.

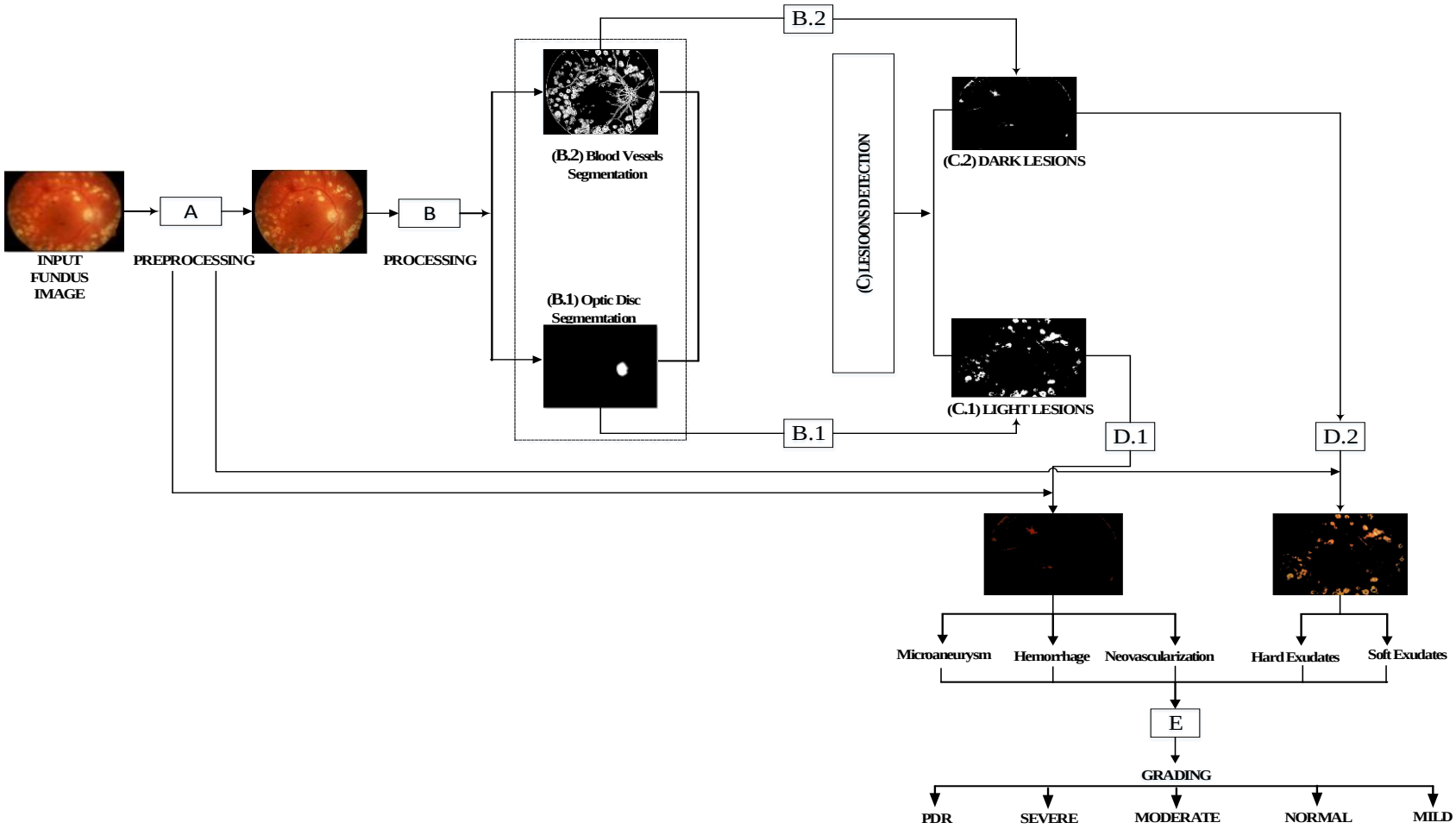

Figure 15: Architecture of the proposed algorithm

3.1 Stage A: Preprocessing

As shown in Figure 15, the preprocessing step is itemized as B. The input of this step is the original RGB retina image (depicted in the step A). The output of this step is the noise free fundus image (depicted in the step B). In retinal imaging, some artifacts can cause noisy recording of fundus images such as illumination or uncalibrated imaging environment. The fundus images may contain unreliable regions because of these artifacts. Using a binary mask, noisy regions can be masked from input images. By using this mask, the areas with sufficiently small level of distortion are only kept. Pseudo code of this stage is shown in Algorithm 1.

The input to the Algorithm 1 is the original fundus image $\boldsymbol{I}$ and the output is noise free image $\boldsymbol{I_m}$.

Algorithm 1. Preprocessing

Input: I (Original RGB fundus image), M (Binary mask)

Output: I_m (Noise free RGB fundus image)

1. Separate R, G and B planes of I obtaining I_r, I_g, I_b
2. Multiply by mask M:

$$I_{rm} = I_r * M$$

$$I_{gm} = I_g * M$$

$$I_{bm} = I_b * M$$

3. Concatenate masked channels: $I_m = cat(3, I_r, I_g, I_b)$

The first step of the algorithm is separating R, G and B channels. In the second step, the mask is multiplied by each channel. After computing masked planes, the last step is concatenating them to produce noise free color image. Figure 16 shows the flow diagram of the preprocessing stage.

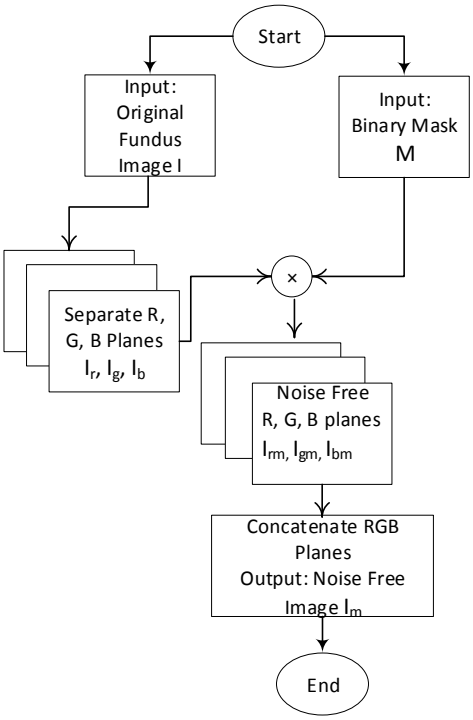

Figure 16: Flow diagram of the preprocessing stage

3.2 Stage B: Processing

As we mentioned before, the segments which are to be seperated include *optic disk*, *blood vessels*, *dark lesions* and *light lesions*. The processing stage (Stage C) of the Figure 15 depicts the detection and mask operation of the *optic disk* and *blood vessels* segments from the noise-free retina images (from Stage B). Creation of *optic disk* mask and detection of *blood vessels* are explained in the following sections. These two segments are detected in this stage before other lesions types because they mislead the system when detecting other lesions.

3.2.1 Stage B.1: Optical Disk Segmentation

Optic Disk (OD) is a circular light pattern in fundus images containing a network of thick blood vessels. When a color fundus image is converted to *black* and *white* to seperate **light lesions** such as *hard exudates* and *soft exudates (or cotton wools)*, this part acts as a disturbing pattern which can be detected mistakenly by the algorithm as

light lesion. In short, the OD can be mistakenly perceived as a light lesion by the algorithm. Therefore, in the first step of the Stage C in Figure 15, the OD is set and a black and white mask is produced to remove the OD from image.

As stated in the previous chapter, different algorithms have been suggested in the literature to find the location of the OD. In this study, we applied a template-based algorithm proposed in [22]. In this method, a template histogram for the OD is constructed in advanced based on characteristics of a rectangular patch containing the OD. More precisely, an average color image of the OD is assumed and histograms of all three channels (i.e. red, green and blue) are extracted.

A fundus image is firstly filtered by an average filter to remove sharp edges and smooth regions. However, as fundus images are in RGB format, each channel needs to be filtered separately. In this study, size of the averaging filter used is equal to 31×31 and its equation (Eq.1) is given as follows:

$$Z = \frac{1}{961}\sum_{i=1}^{961} F_i \qquad (1)$$

where F_i is the original pixel value in a gray-scale image (red, green or blue channels) and Z is the related pixel value in averaged image. A better representation of average filtering is illustrated in Figure 17.

	1	2	...	30	31
1	1/961	1/961	...	1/961	1/961
2	1/961	1/961	...	1/961	1/961
⋮	⋮	⋮	...	⋮	⋮
30	1/961	1/961	...	1/961	1/961
31	1/961	1/961	...	1/961	1/961

Figure 17: Average filtering

Then the image is searched from the top left corner to the bottom right corner to find a patch with is most likely to contain OD. In other word, image is converted into rectangular blocks of fixed size and via an iterative scheme, histogram of each block is compared to the template histogram. The size of the blocks, $\boldsymbol{n}$, is data dependent and need to be defined by practice. The aim is to find the block with maximum similarity score of histogram with the template histogram. Calculation of similarity score is as follows. Firstly, a block of size $\boldsymbol{n}\times\boldsymbol{n}$ is selected from each of the average images in red, green and blue planes. Histogram is calculated and a correlation coefficient is assigned to each of them according to the following formula (Eq. 2).

$$C_p = \frac{1}{1 + \sum(T_p - I_p)^2} \tag{2}$$

where $\boldsymbol{p}$ is either $\boldsymbol{r}$ or $\boldsymbol{g}$ or $\boldsymbol{b}$ representing *red*, *green* or *blue* channel. $\boldsymbol{T_p}$ is the histogram of the template plane and $\boldsymbol{I_p}$ is the histogram of the selected block for the same color plane.

In this stage, three correlation coefficients, namely $\boldsymbol{C_r}$, $\boldsymbol{C_g}$ and $\boldsymbol{C_b}$ are obtained. The similarity score is the weighted sum of these three coefficients. It should be noted that contribution of the color planes in contrast of the OD image is not similar. In fact, this

is highest for green, moderate for blue and lowest for red. Consequently, the weights are defined as 2, 1 and 0.5 for each of the separately. We call these weights ***g***, ***b*** and ***r***. Finally, the total similarity score is computed as stated in the following formula (Eq.3).

$$C(i,j) = r * C_r + g * C_g + b * C_b \quad (3)$$

The pixel with ***maximum*** value of ***C(i,j)*** is the location of optical disk.

Algorithm 2 explains the procedure of OD detection briefly. The flow diagram of OD segmentation method is also shown in Figure 18.

The input to this algorithm is noise free color image (I_m) and the output is binary OD mask (I_{OD}). As explained before, the first step is computing average image I_z. In the second stage, the procedure of computing ***C(i,j)*** is applied on all patches. OD location is detected in the third step as the argument of maximum ***C*** value. After locating OD, Otsu's method [28] is utilized to convert I_m into black and white image in the fourth step. The threshold varies from on image to another one. After calculating black and white I_{BW}, region of OD is separated by using the found OD location.

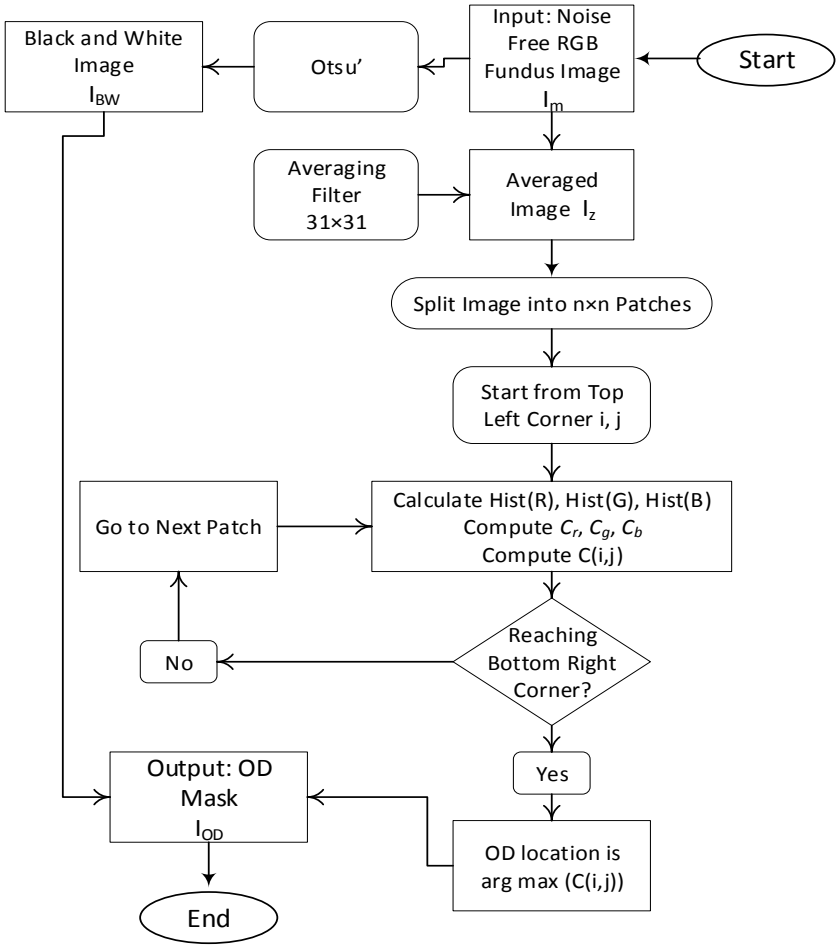

Figure 18: Flow diagram of OD segmentation

Algorithm 2. OD Mask

Input: I_m (Noise free RGB fundus image)

Output: I_{OD} (Binary OD mask)

1. Apply averaging filter (Eq. 1) on I_m to obtain I_z
2. For all "n×n" patches of I_z:

   Calculate histogram of R, G and B planes

   Compute C_r, C_g, C_b using Eq. 2

   Compute C (i,j) based on Eq. 3
3. Find OD (i, j) = arg max {C}
4. Apply Otsu's method [28] on I_m to get black and white image I_{BW}
5. Separate region that contains OD (i,j) to produce the OD (I_{OD})

3.2.2 Stage B.2: Blood Vessels Segmentation

The appearance of *Blood Vessels (BV)* in retina images is *linear*. The network of connected red lines with variable thickness is required to be detected and removed from the fundus images. In fact, *intensity* or *gray scale value* of the BV is very close to *dark lesions* such as the H or the MA. Hence, it is necessary to detect the BV with acceptable accuracy. As mentioned in Section 2.3, different algorithms have been applied on fundus images to detect the BV. All methods are trying to enhance edges in the image in all the directions since the network of BV has distributed unevenly in different directions.

One of the well-known methods for edge detection in images is ***Kirsch method*** which is explained in the previous chapter. This method is implemented quickly and detects edges even when the BV are thin. Kirsch method is applied by using 8 filters in 8 different angles to retinal images. In the first stage, input RGB image is converted to a gray scale image. Then, Kirsch template filters are applied one by one to the fundus image. In this step, eight images are obtained in each of them edges are enhanced in a specific direction.

Filters contains a set of 8 edge enhancers starting from 0 and adding 45 degrees as proceeding to the other one. The directions are 0, 45, 90, 135, 180, 225, 270 and 315 degrees in the 360 plane. In order to detect edges from these filtered images, a predefined threshold value is required. The value of this Kirsch threshold is a number between 1 to 15 and varies remarkably from one data to another.

The related pixels amongst all edge-enhanced images are compared and the maximum value found is kept. In other words, a single pixel added to blood vessels' mask when

its maximum value among all 8 images is larger than threshold. The threshold value is set as '3' in this study according to practical evaluations on the selected data set. The pseudo code of the method is given in Algorithm 3.

Algorithm 3. Blood Vessel Segmentation

Input: I_m (Noise free RGB fundus image), Threshold = 3

Output: I_{BV} (Binary blood vessels mask)

1. I_{BV} = zeros(size(I_m))
2. Convert I_m to gray scale image $\mathbf{I_{gray}}$
3. Apply 8 Kirsch filters to obtain $\mathbf{\{I_1, I_2, ... I_8\}}$
4. For each pixel location (i,j)

   Find M(i,j) = max{I_1(i,j), I_2(i,j), ... I_8(i,j)}

   If M(i,j) > Threshold, I_{BV}(i,j) = 1

The input to the algorithm is noise free fundus image $\boldsymbol{I_m}$ and the output is *black* and *white* BV mask $\boldsymbol{I_{BV}}$. The first step of this algorithm is to initialized BV image as a *zero* image. In the second step, conversion of the noise-free RGB fundus image (from Stage B) into gray scale is performed. The third stage is applying the Kirsch filtering. Kirsch template filters (uses these angles for directions that are 0, 45, 90, 135, 180, 225, 270 and 315) are applied one by one to the fundus image. In this step, eight images are obtained $\boldsymbol{\{I_1, I_2, ... I_8\}}$. In the fourth step, the maximum value of each separate pixel locations ***(i, j)*** of the eight filtered images $\boldsymbol{\{I_1, I_2, ... I_8\}}$ are found. Then, the maximum value found is compared with a threshold (is taken as 3) in the same step. The pixel value of $\boldsymbol{I_{BV}}$ for each the maximum value is above threshold is set to ***'1'*** in order to produce the mask. For better understanding, the flow diagram of the used BV detection is also illustrated in Figure 19.

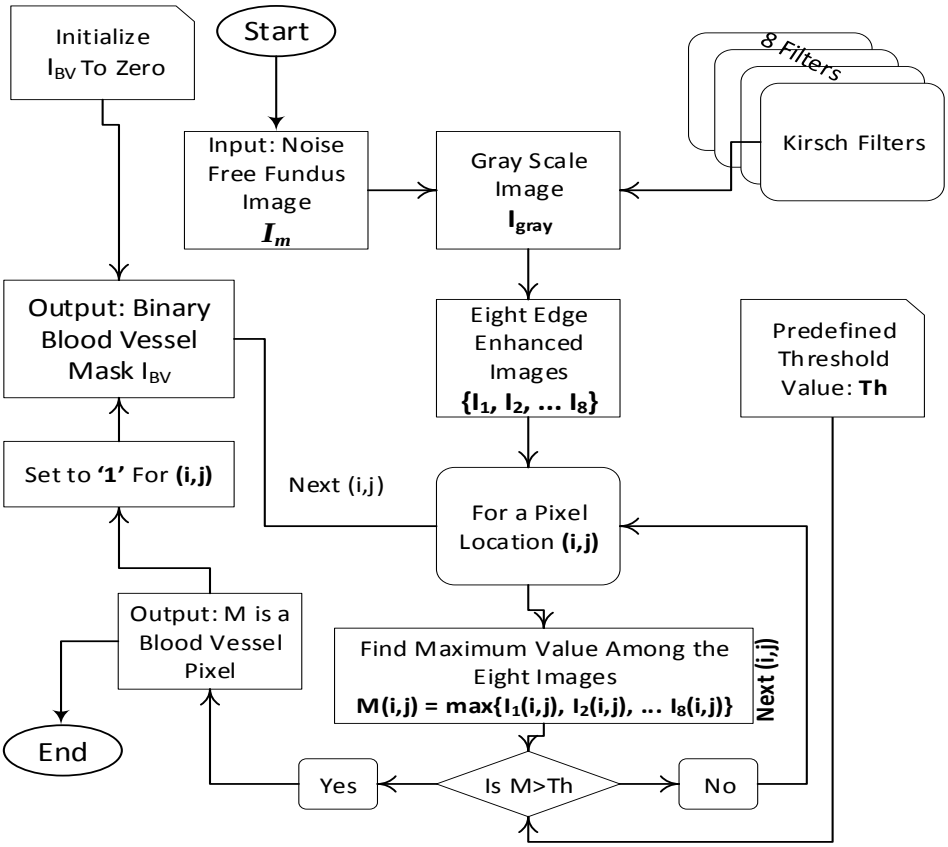

Figure 19: Flow diagram of blood vessel segmentation

3.3 Stage C: Lesion Detection

In lesion detection phase named as (Stage D) in Figure 15, there are two parallel steps to distinguish for *Light Lesions* (Stage E) and *Dark Lesions* (Stage F). In this step, firstly OD and BV are to be masked from images. The created black and white masks as output have value equal to 255 or logical one (white) in related regions and are equal to 0 or logical zero (black) in desired area. Hence, OD and BV masks are required to be complemented or in other words be converted into negative images.

For example, if we want to mask OD from an image, we need a mask which is black in OD region and white in other parts. Negative masks are created by taking the logical complement of black and white images. This is also possible to convert them into b-

bit unsigned integers (value 0 and 255) and subtract 255 from the original mask to produce a negative mask. Once producing these masks for OD and BV, each color plane can be simply multiplied by mask. At the end, mask RGB channels are concatenated to produce a masked color image.

After masking OD and BV from images, the next stage is *Lesions Detection* which involves *Light Lesion* and *Dark Lesion segmentations*. In Algorithm 4, these segmentation procedure are represented as pseudo code. The inputs of the algorithm are $\boldsymbol{I_m}$, $\boldsymbol{I_{OD}}$ and $\boldsymbol{I_{BV}}$. The outputs are the ***types of lesions (MA, H, NV, HE, SE)***. The first step is segmentation of dark lesions.

The details are explained in the following paragraphs. The output of the first step of Algorithm 4 is a color image of segmented dark lesion. The second step follows a similar procedure to produce a color image of segmented light lesions. In the third step, six features are extracted from each segmented region as described before. The fourth step includes SVM training and testing. Finally in the fifth step, lesion types are detected.

3.3.1 Stage C.1: Light Lesions Detection

As mentioned previously, *Light Lesions* contain red small dots or **HE** and **SE** (or **CWS**) as shown in Figure 15 (depicted Stages H and G). The procedure of light lesion detection is summarized in Figure 20 as a flow diagram. A similar procedure is applied to segmentation for both light and dark lesions. As shown in Figure 20, the input to the algorithm is noise free fundus image $\boldsymbol{I_m}$ and the output is **HE** and **SE** (or **CWS**) detected lesion types.

Algorithm 4. Lesion Detection

Input: I_m (Noise free RGB fundus image), I_{OD} (OD mask), I_{BV} (Blood vessels mask)

Output: Lesion type (MA, H, NV, HE, SE)

1. Segmentation of dark lesions
   - Separate green plane of I_m: I_g
   - Compute image complement: $I_{comp} = 255 - I_g$
   - Apply Otsu's threshold on I_{comp} to produce black and white image I_{dark}
   - Mask BV by $I_{dark} = I_{dark} \times I_{BV}$
   - Separate R,G, B planes of I_m: I_r, I_g, I_b
   - Produce color segments $I_{darkRGB} = \text{cat}\{I_r \times I_{dark}, I_g \times I_{dark}, I_b \times I_{dark}\}$
2. Segmentation of light lesions
   - Convert I_m to gray scale image: I_{gray}
   - Apply Otsu's threshold×2 on I_{gray} to produce black and white image I_{light}
   - Mask OD by $I_{light} = I_{light} \times I_{OD}$
   - Separate R,G, B planes of I_m: I_r, I_g, I_b
   - Produce color segments $I_{lightRGB} = \text{cat}\{I_r \times I_{light}, I_g \times I_{light}, I_b \times I_{light}\}$
3. Extract six features from all segments in $I_{darkRGB}$ and $I_{lightRGB}$
4. Classify features by SVM (SVMlight library)
5. Detect lesion type for each segment: MA, H, NV, HE or SE

Steps are: 1) the gray-scale fundus image is masked by OD mask instead of BV, 2) Otsu's method is applied on gray-scale image and not just green channels, and 3) there is no need to produce negative image since HE and CWS have generally larger intensity and pixel value in the image. According to our investigations, Otsu's threshold should be multiplied by 2 to produce an acceptable mask for light lesions. The mask is applied on red, green and blue planes separately and then they are concatenated to produce a colored segmented image (Figure 15 parts 12 to 15).

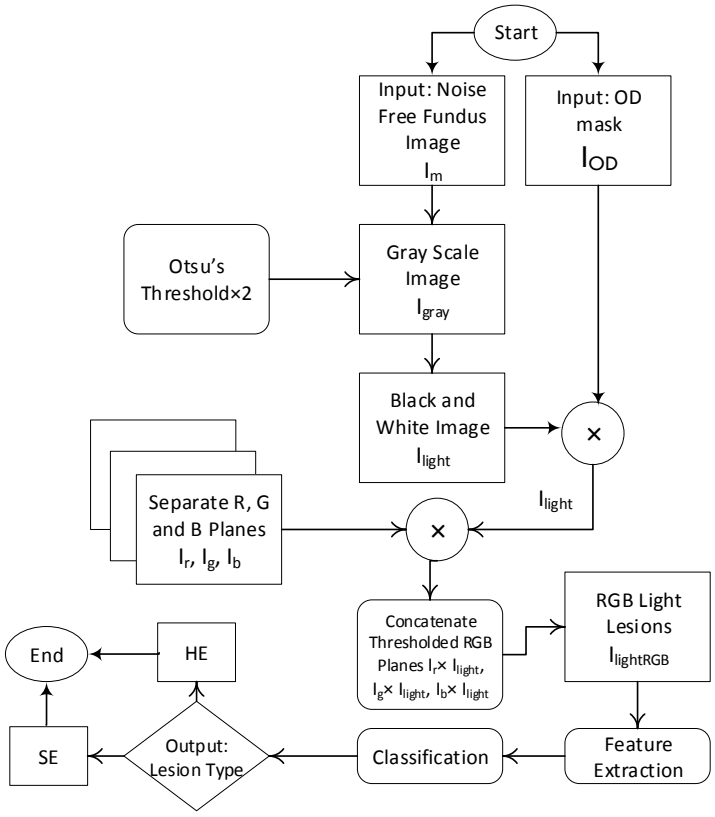

Figure 20: Flow diagram of light lesion detection (HE and SE)

After segmentation, feature selection is applied to extract features from each segmented area. Six features are extracted from each lesion including: ***area***, ***eccentricity, mean gradient, mean hue, mean value*** and ***mean saturation***. These features contain descriptive information about ***size, form, color*** and ***brightness of lesions*** which is crucial for detection of anomalies.

Area is defined as the number of pixels in the segmented region. ***Eccentricity*** is a value between 0 to 1 that shows how round-shaped a segment is. For a linear segment this feature is 0 and for a circle it is equal to 1. ***Mean gradient*** is the average of gradient magnitude of pixels in the region. ***Mean hue***, ***mean value*** and ***mean saturation*** are calculated by converting RGB image into HSV image.

Features are extracted to train and test a classifier. In this study, linear SVM classifier is used which is a powerful and well-known classifier in image processing and machine leaning community. The library of ***SVMlight*** [29] is utilized for implementation. Text and train data are selected based on ***5-fold cross validation*** method. In this method, the whole data set is divided into 5 partitions. Each time one partition is taken out for testing and the remaining partitions are used for training classifier. This procedure is repeated 5 times and performance metrics are computed.

3.3.2 Stage C.2: Dark Lesions Detection

As mentioned previously, *Dark Lesions* include red small dots or ***MA, H,*** and ***NV*** as shown in Figure 15 (depicted in Stages K, J, and I). To separate these type of lesions, we focus on ***green channel*** for threshold selection. The reason of this, all these type of lesions are related with bleeding and BV, and are clearer (appear clearly) in green plane. The process is shown as a flow diagram in Figure 21 and explained in details in the following paragraphs.

At first, RGB retinal image is converted into gray-scale image. This image is complemented by subtracting 255 from pixel values. Dark lesions in the complemented image have larger pixel values. Then, BV mask is applied to suppress the pixel values related to them to zero. In this step, a threshold is needed to produce black and white image. This threshold is calculated from green plane as explained before. Otsu's method is used for threshold selection [28]. This method finds a threshold that reduces the intra class variance of black and white pixels using histogram. Otsu's threshold is applied and gray-scale image is converted into black and white in a way that darker lesions are separated from other parts. This mask is applied to all three color planes, they are concatenated and a colored segmented image is produced.

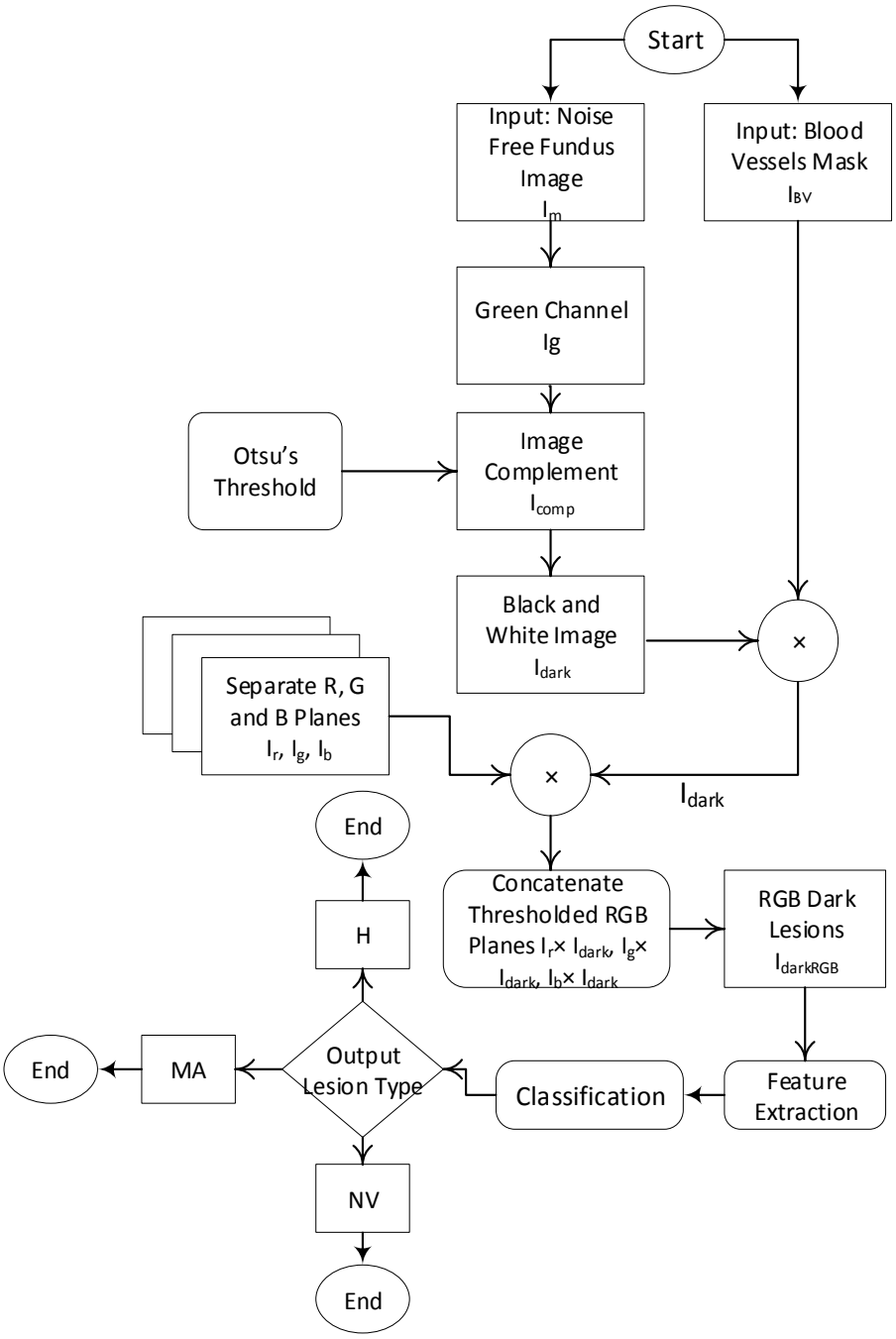

Figure 21: Flow diagram of dark lesion detection (MA, H and NV)

Similar to light lesion detection, SVM classifier is applied to discriminate between three types of dark lesions. Again, train and test sets are prepared based on ***5-fold cross validation*** method. As the number of classes are more than two here, including MA, H and NV, two levels are two-class SVMs are applied. Details of classification stage have been explained in chapter four.

3.4 Stage E: Grading

The final step of the work is to roughly define a scale for severity of the disease in each image which contains detected signs of DR as shown in Step 16 of the Figure 15. This part cannot be performed simply because GT file does not contain enough information about it. However, we have implemented a simple grading system based on Table 1. A rule-based code has been written which assigns a severity level to each image. The GT file provided beside the data set is also used in the same fashion to produce a GT for severity scale. In this final step, each image in the data set have a detected level and a GTlevel. By comparing this two, performance of our grading system is measured. Algorithm 5 shows a pseudo code of grading. Inputs of the algorithm are the lesion types detected in the previous phase. The output is the severity grade of the DR disease. The first step of the Algorithm 5 checks if there is any abnormality. If not, there is a normal fundus image. Secondly, if there are just signs of MA and not any others, the grade is mild. For the third step, MA may appear with any other abnormality at the same time which is moderate level. If there is any sign of NV, the grade is PDR. The default case is the severe level.

Algorithm 5. DR grading

Input: Lesion types in an image (MA, H, NV, HE, SE)
Output: DR grade (normal, mild, moderate, severe, PDR)

```
If !{MA, H, NV, HE, SE}
        DR grade = normal
    Else if MA & !{H, NV, HE, SE}
        DR grade = mild
    Else if {MA & H} or {MA & HE} or {MA & SE} & !NV
        DR grade = moderate
    Else if NV
        DR grade = PDR
    Else
```

DR grade = severe

Table 3 shows some results of considered images as example (see Appendix B for whole images). Detected lesions and assigned severity scales are shown in the Table 3. In order to have a comparative perspective, the same rule-based approach is also applied on (GT) file (see Appendix B for whole images).

Table 3: Detected lesions and grade for first 10 images

Image No.	**Detected Abnormal Lesions**					**Detected Grade**	**GT Grade**
1	MA	H	HE	n/a	n/a	severe	Severe
2	MA	H	HE	n/a	n/a	severe	Severe
3	n/a	n/a	HE	SE	n/a	severe	Severe
4	MA	H	n/a	n/a	n/a	moderate	Severe
5	MA	n/a	n/a	n/a	n/a	mild	Severe
6	MA	H	n/a	n/a	n/a	moderate	Severe
7	MA	H	HE	SE	n/a	severe	Severe
8	MA	H	HE	n/a	n/a	severe	Severe
9	MA	H	HE	SE	n/a	severe	Severe
10	n/a	H	n/a	SE	n/a	Severe	Severe

Chapter 4

METHODOLOGY

4.1 Databases

Four data sets are selected to be used in this study. DIARETDB0 is a data set of color fundus images [10]. The data is publically available and corresponds to practical situations. The images have taken with several fundus cameras containing different amounts imaging noise and optical aberrations, hence it is referred to as "calibration level 0 fundus images". The data set can be used to evaluate the general performance of diagnosis methods. The data set contains 130 images of which 110 have signs of anomalies related to DR. In other words, 110 images contain signs of red small dots, H, HE, CWS or MA while 20 of them are normal with no sign of DR. Images were captured with a 50 degree field-of-view digital fundus camera with unknown camera settings. The data correspond to practical situations, and can be used to evaluate the general performance of diagnosis methods. This data set is referred to as "calibration level 0 fundus images".

In addition to the images, a folder containing valid area mask is also provided. These masks are black and white images to remove noisy parts and background from retinal images. In this study, removing noisy region is part of the preprocessing by multiplying these masks with the original images. It should be noted that except for a few cases, valid area includes the whole image and preprocessing does not change the

details so much. Figure 22 shows two example fundus images, their binary masks and resulted noise free images.

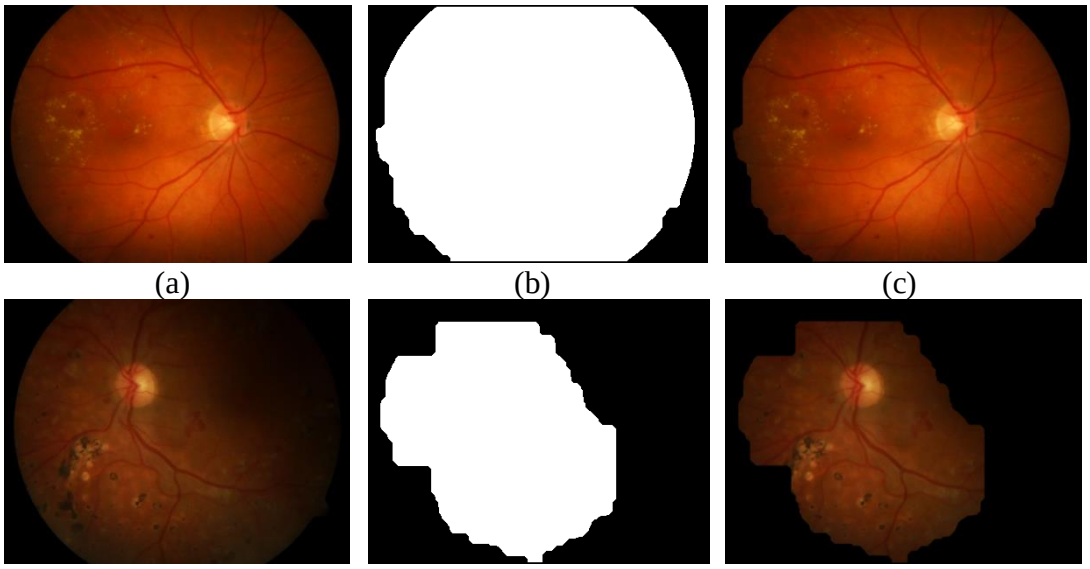

Figure 22: Removing noisy region
(a, d) Original fundus image
(b, e) binary noise removal mask
(c, f) noise free image

Another important information available by this data set is the GT file. GT has been prepared by medical experts. For each image, a text file is available containing five entries each of them pointed to one of the five types of anomalies which may appear in fundus images of patients suffering from DR. If a specific anomaly does not exist, its related entry is registered as 'n/a'. If it does, the name of it i.e. H, HE, or NV etc. is written there. We have merged all these text files in one cell array of 130 rows and 5 columns. This is called the text label file. The GT file is available in Appendix A.

Another data set used in this work is DIARETDB1 data set [11].The data correspond to a good (not necessarily typical) practical situation, where the images are comparable, and can be used to evaluate the general performance of diagnostic

methods. The general performance corresponds to the situation where no calibration is performed (actual physical measurement values cannot be recovered), but where the images correspond to commonly used imaging conditions, i.e., the conditions encountered in hospitals. This data set is referred to as "calibration level 1 fundus images". The database consists of 89 colored fundus images of which 84 contain at least mild nonproliferative signs (MA) of DR. The images were taken in the Kuopio university hospital. The images were selected by the medical experts, but their distribution does not correspond to any typical population, i.e., the data is biased and no a priori information can be devised from it. The diabetic retinopathy abnormalities in the database are relatively small, but they appear near the macula which is considered to threaten the eyesight.

Images were captured with the same 50 degree field-of-view digital fundus camera with varying imaging settings (flash intensity, shutter speed, aperture, gain) controlled by the system. The images contain a varying amount of imaging noise, but the optical aberrations (dispersion, transverse and lateral chromatic, spherical, field curvature, coma, astigmatism, distortion) and photometric accuracy (color or intensity) are the same. Therefore, the system induced photometric variance over the visual appearance of the different retinopathy findings can be considered as small. Because of this calibrated non-changing setting, there is one standard mask for all the images. Hence, the procedure of valid area detection by noise removal mask is not applicable [11].

The HRF database [13] has been established by a collaborative research group consisting of two European institutions: Brno University of Technology, Faculty of Electrical Engineering and Communication, Department of Biomedical Engineering, Brno, Czech Republic, and Pattern Recognition Lab at the University of Erlangen–

Nuremberg, Germany. The goal of this dataset is to support comparative studies on automatic segmentation algorithms on retinal images, especially high-resolution ones. This database contains three sets of fundus images: healthy retinas, glaucomatous and DR retinas. The total number of images is 45 and there are 15 images for each category. Binary adjustment masks are also provided for each image to remove background. In our study, we used 15 normal and 15 DR images of HRF data set. Since this data set is published mainly for blood vessel segmentation, there is no GT file for this data set containing lesions and anomaly types. As a result, it is not possible to evaluate the performance of the whole system on it. We only evaluate the performance of the system on DR detection on this data set [13].

STARE is another well-known colored fundus image data set which is publically available [12]. This data set is prepared aligned with STARE (STructured Analysis of the Retina) Project. STARE was conceived and initiated in 1975 by Michael Goldbaum, M.D., at the University of California, San Diego. It was funded by the U.S. National Institutes of Health. During its history, over thirty people contributed to the project, with backgrounds ranging from medicine to science to engineering. Images and clinical data were provided by the Shiley Eye Center at the University of California, San Diego, and by the Veterans Administration Medical Center in San Diego [12]. An ophthalmologist who is known as a medical doctor that specializes in the structure, function, and diseases of the human eye has noted the findings of each recorded image. The ophthalmologist then uses these findings to reason about the health of the subject. For instance, a patient may exhibit discoloration of the optic nerve, or a narrowing of the blood vessels in the retina. An opthalmologist uses this information to diagnose the patient, as having for instance Coats' disease or a central retinal artery occlusion. STARE data set includes about 400 colored fundus images in

.ppm format. The GT file is a text file with different diagnoses and diagnoses codes. For example '0' is the code for a normal image and '7' is for DR. As the data contains many images with different illnesses, we have to select a subset suitable for this study. By analyzing the diagnosis codes, it was observed that there are 58 normal subjects and 67 DR subjects in data set. A subset of 40 images has been selected for this study including 20 normal and 20 DR subjects. To summarize the information about data sets, Table 4 is prepared. Number of images in each category is shown in the table. the '#' sign stands for 'number of'.

Table 4: Data set description

Data set	Total	#Normal	#DR	Selected N/DR
DiaretDB0	130	20	110	20/110
DiaretDB1	89	5	84	5/84
STARE	~400	58	67	20/20
HRF	45	15	15	15/15

4.2 Support Vector Machines

The problem of the classification has been performed using SVMlight library [29]. It is a popular open source machine learning library which is optimized for CPU and memory. SVMs are usually adapted for the purpose of data classification. Most probably, in any classification problem the data is separated into training and testing sets. Each example in the training set contains a class label and several features. Based on the training data, the objective of SVM is to produce a model which is able to estimate the target values of the test data given only the test data features. Assume a training set of instance pair of labels (x_i, y_i), $i = 1, 2, \ldots, l$ where $x_i \in R^n$ is the feature vector and $y \in \{1, -1\}$ is the class label such that $y = +1$ for positive samples and $y = -1$ for negative samples [30]. Figure 23 shows an example in two dimensional feature

space in which circles belong to class 1 and rectangles belong to class 2 samples. Linear SVM which is utilized in our study, solves a Lagrange optimization problem to find the optimal hyperplane with maximum distance from closest samples. These samples are named support vectors. Hence, when SVM is training, it finds support vectors to build the optimum separating hyperplane for discriminating positive samples from negative ones.

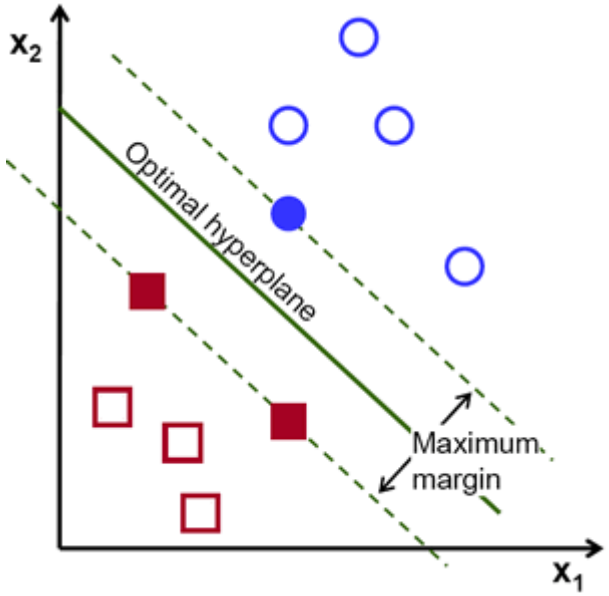

Figure 23: SVM optimal hyperplane

SVMlight is an implementation of Support Vector Machines (SVMs) in C. This is based on is Vapnik's Support Vector Machine [30] for the problem of pattern recognition, for the problem of regression, and for the problem of learning a ranking function. The optimization algorithm used in SVMlight is described in [31]. The algorithm has scalable memory requirements and can handle problems with many thousands of support vectors efficiently. The software also provides methods for assessing the generalization performance efficiently.

4.3 5-Fold Cross Validation

Cross validation is a technique and sometimes it's called rotational estimation. The whole dataset we called D, was randomly divided to number of fold (divided to K), then we have K subset (D_1, D_2, …, D_K) with approximately same size. For the K-fold cross-validation, the initial starting sample is subdivided into approximately K equal size subsamples in a random manner. A single subsample is retained in the K subsamples in order to validate data that will test the model and the left out K-1 subsample will be used as training data. The K subsamples are used exactly once as the validation data right after the cross-validation process is set out to run k times repeatedly. A single estimation is presented after a computation of the K-fold average to give the outcome of K-result. All observations are used for both training and validation and therefore this serve as a primary advantage of this method and will then be used for validation just only once.

Using stratified K-fold cross-validation allows each fold to consist of only similar sizes and proportions of class labels and that mitigates classification problems. The cross-validation procedure is to be repeated n times in repeated cross-validation process to give n random partitions of the original sample. A single estimation is produced when the n results are averaged. For example, we consider K equal to 5 and then we have a dataset that is randomly separated into 5 similar folds of equal sizes generated by K equal that gives us 5-fold CV. Each run consist of 4 subdivisions that are utilized primarily for training set and the last subset is used for validation (see Figure 24). After each repetition of 5 runs during the procedure, each subset is only used once for validation. After the system has completed running, all the 5 validated results are combined together with the primary purpose of creating an individual of a calculation

of out-of-sample. The K-fold CV obtained a generalization error and K was then wound to 5 in order to balance calculation costs and reliable estimates and to fairly compare with the state of the art.

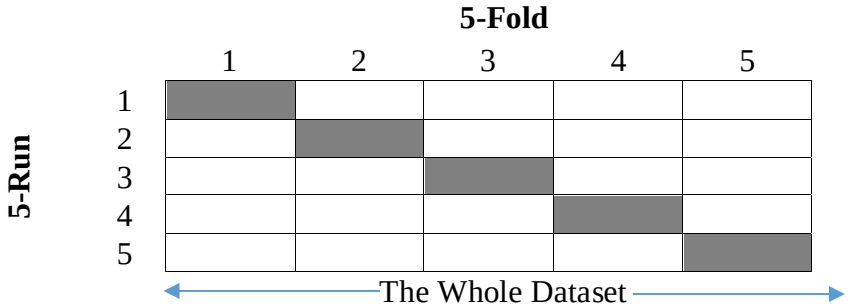

Figure 24: 5-fold cross validation data split

4.4 Case Study on DIARETDB0

As explained in detail in previous chapter, the proposed method starts with finding the location of OD. For this purpose, firstly an average filter of size 31x31 is applied. Then, a template-based method based on histogram is used to find the location of OD. Size of the patches (n×n) for OD detection is set to 130×130 according to the primary evaluations on data set. It should be noted that there are a few images in the data set in which OD does not appear as shown in Figure 25. The algorithm fails in these cases. According to our investigations there are two images with no observable OD region. For other cases the algorithm accurately finds more than 96% of ODs.

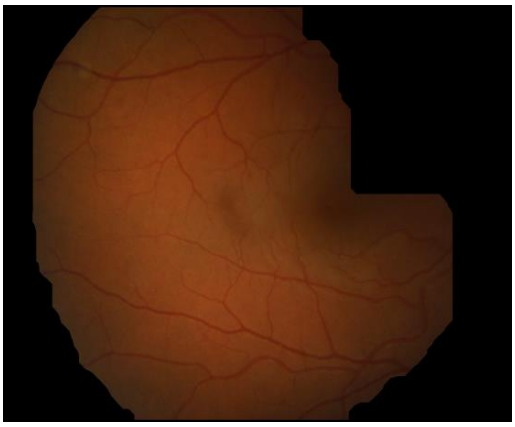

Figure 25: An example image with no OD

The procedure of finding the location of OD is followed by converting the images into black and white image using Otsu's threshold [28]. The related segment that contains the pixel of location of OD is picked to produce a binary OD mask. Figure 26 represents a sample image and detected OD location. In Figure 27, OD mask is shown.

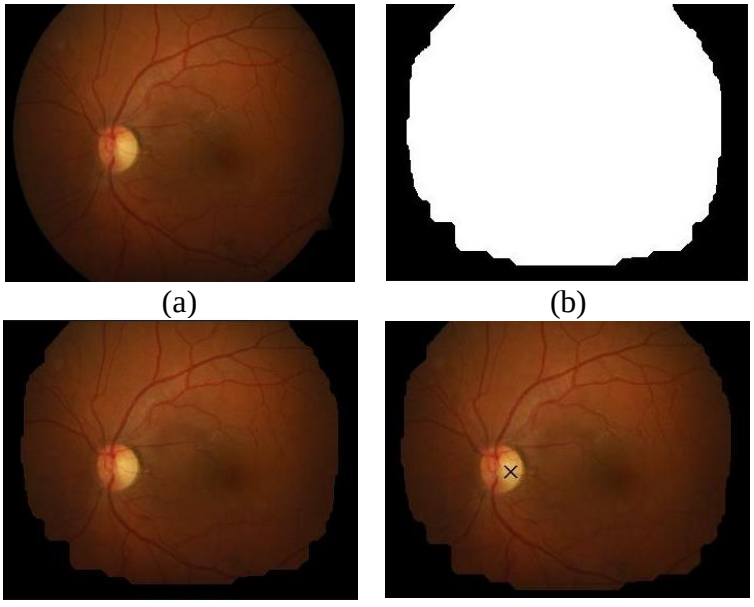

(a) (b)

(c) (d)

Figure 26: Finding the location of OD
(a) Original image
(b) Valid binary mask
(c) Applying valid binary mask
(d) Detection of OD

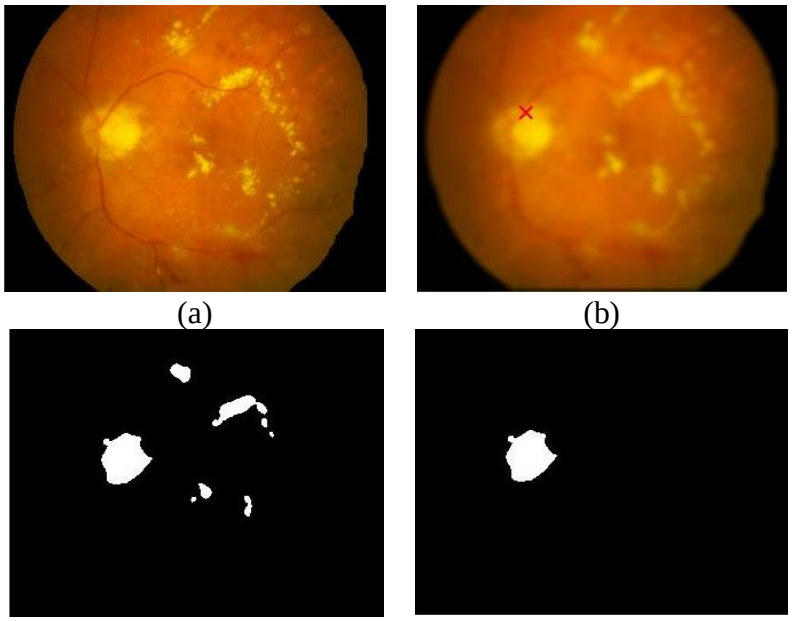

(a) (b)

(c) (d)

Figure 27: Producing OD binary mask
(a) Original image
(b) Filtered image (averaging) and detected OD
(c) Thresholded image (d) OD mask

The next step is applying Kirsch method to enhance edges for BVs detection. As explained in previous chapter, Kirsch applies eight filters in eight different angles to capture all BVs spreading in different directions. Figure 28 illustrates the results of edge enhancement using this method. Eight edge-enhanced images are shown. Using these images, a binary image is produced which is shown in Figure 29.

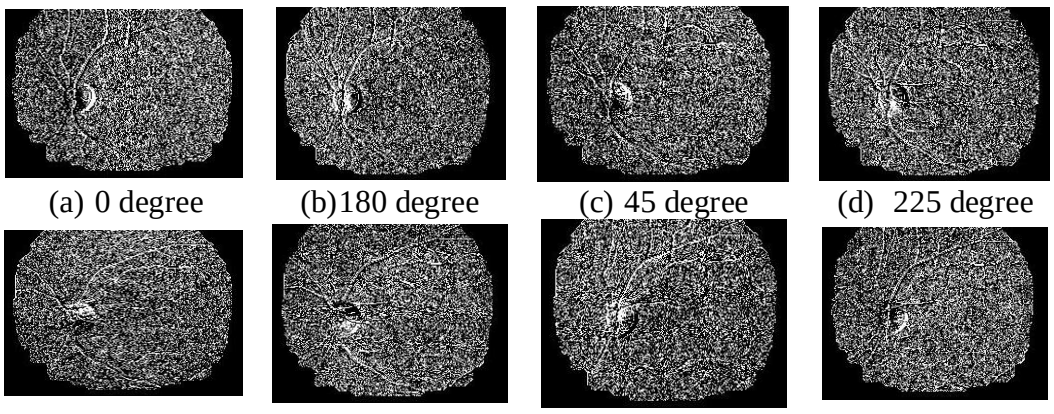

(a) 0 degree (b)180 degree (c) 45 degree (d) 225 degree

(e) 90 degree (f) 270 degree (g) 135 degree (h) 315 degree

Figure 28: Kirsch edge enhanced images

It can be seen that this image contains noisy pixels that do not belong to BVs. The noise is removed from BV mask image by applying a median filter and then removing regions with less than 200 pixels. The value of 200 is calculated by practically investigating different numbers on data set Bhadauria et al. in [18]. The fact behind this is that BVs are connected linear components with many pixels. Hence, any small unconnected region can be considered as noise. Figure 29 and 30 show this procedure.

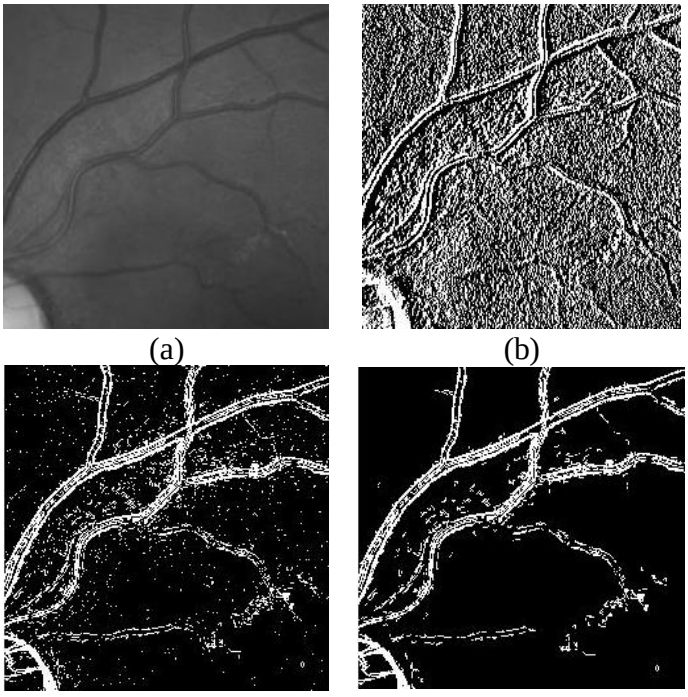

Figure 29: Noise removal from BV mask
(a) Gray scale image (b) Edge enhanced image (0 degree)
(c) Detected blood vessels
(d) Noise removal

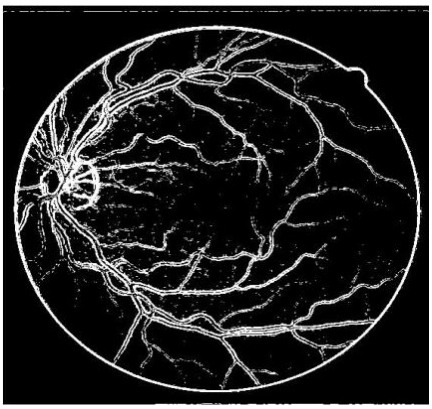

Figure 30: Detected BVs

After producing OD and BV mask, light and dark lesions are segmented in fundus images. The procedure has been explained in Section 3.3 in details. A thresholding method is used based on Otsu's method with some modifications for light and dark lesions separately. The result is illustrated in Figures 31 to 33.

In order to make the result clearer, an image containing red small dots, H and CWS is shown in Figure 34. Original image, segmented light/dark lesions and related anomalies extracted from GT file are clarified. By comparing dark lesions with small dots and H regions, we can see that the system segments this region in dark lesion mask correctly. The same comparison can be seen in light lesion mask and CWS. Another example is shown in Figure 35 for detection of NV. This is important specifically for grading of DR since NV the occurrence of is the most severe level of DR.

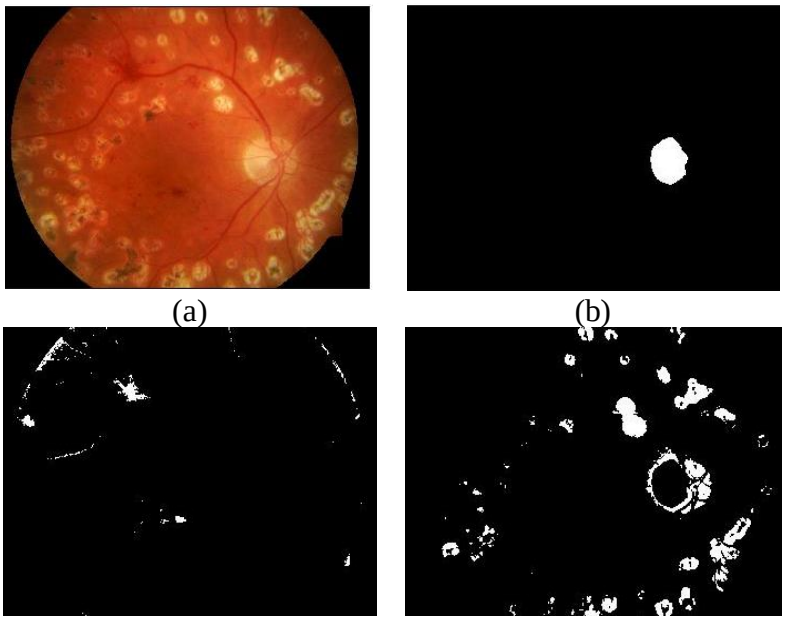

(a) (b)

(c) (d)

Figure 31: Segmentation of dark and light lesions
(a) Original image
(b) Segmented OD
(c) Segmented dark lesions
(d) Segmented light lesions

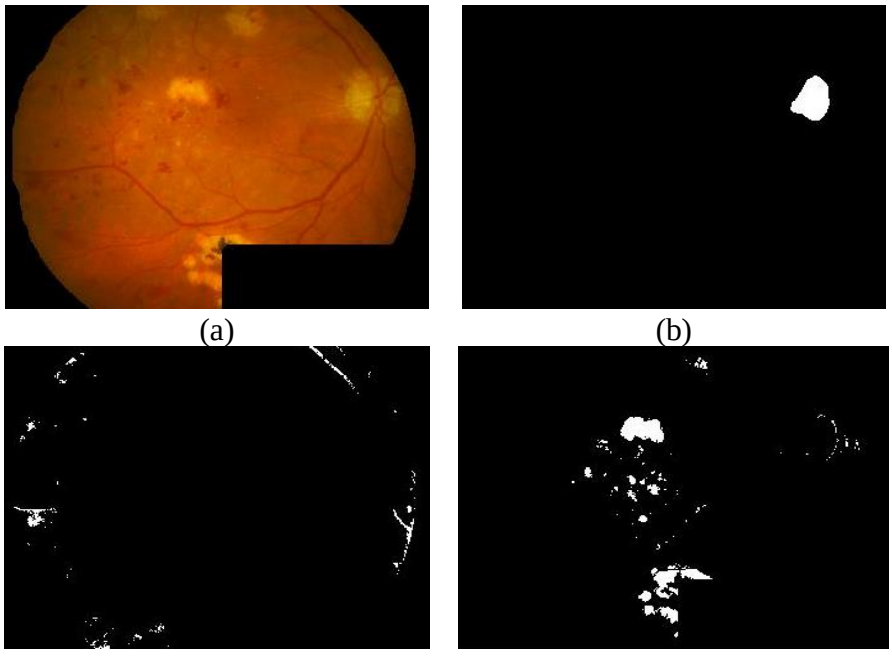

(a) (b)

(c) (d)

Figure 32: Segmentation of dark and light lesions
(a) Original image (b) Segmented OD
(c) Segmented dark lesions
(d) Segmented light lesions

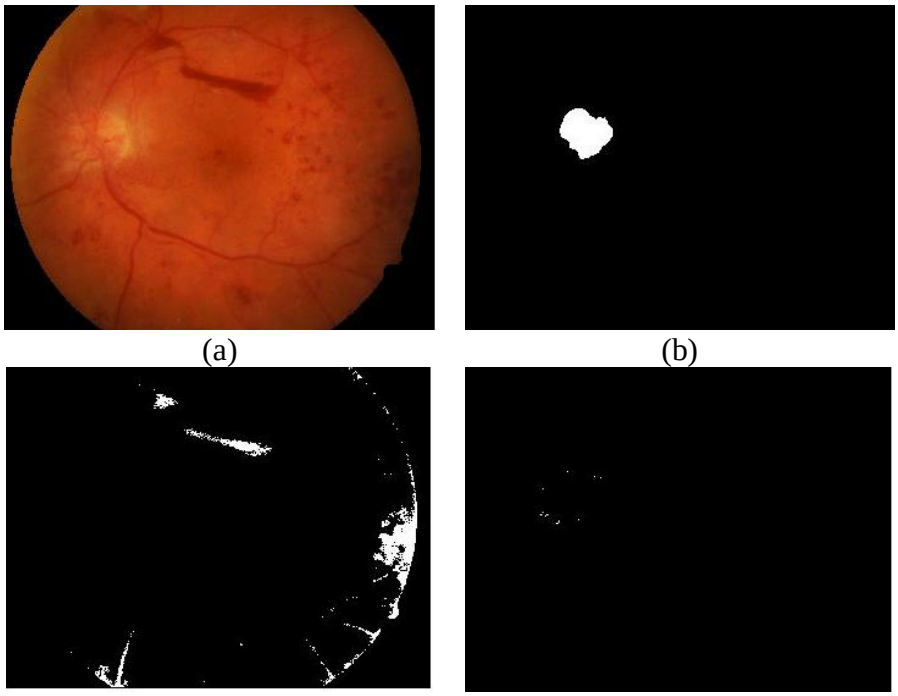

(a) (b)

(c) (d)

Figure 33: Segmentation of dark and light lesions
(a) Original image (b) Segmented OD
(c) Segmented dark lesions
(d) Segmented light lesions

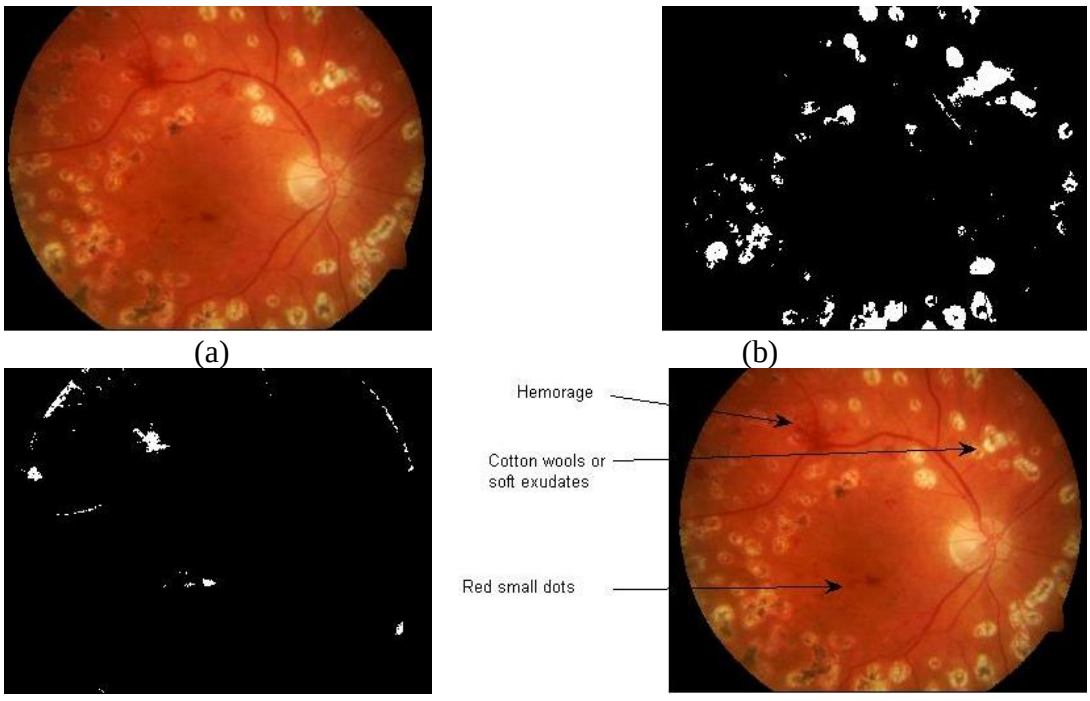

(a) (b)

(c) (d)

Figure 34: Segmentation of dark and light lesions with anomalies from GT
(a) Original image (b) Light lesions
(c) Dark lesions (d) Recognized anomalies

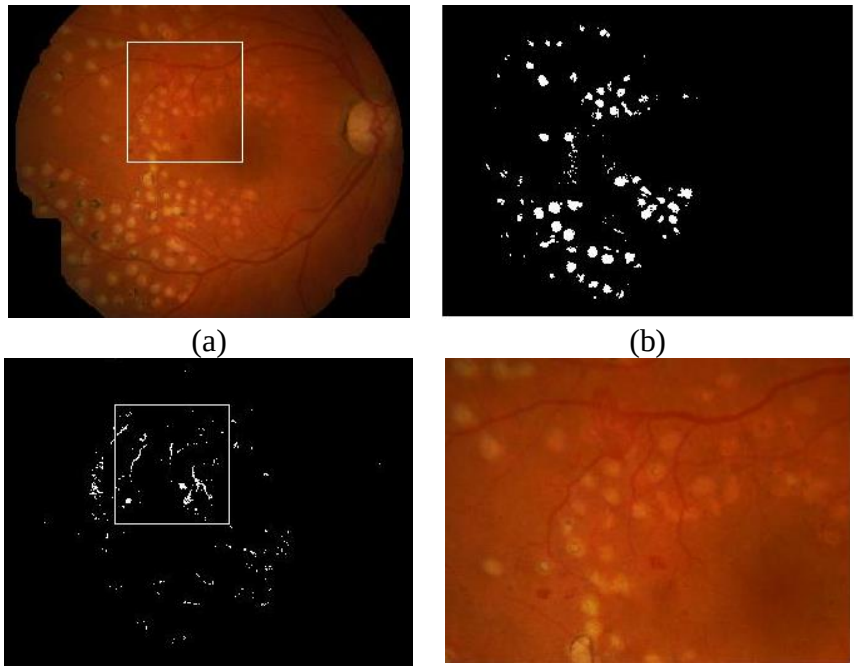

(a) (b)

(c) (d)

Figure 35: Segmentation of dark and light lesions and NV detection
(a) Original image with NV (b) Light lesions
(c) Dark lesions with detected abnormal blood vessels (d) NV area

In this step, light and dark lesions binary masks are applied to images. It should be noted that OD and BVs are already removed from images in this step. The resulted images are RGB color images of segmented dark and light lesions. Figure 36 shows these images.

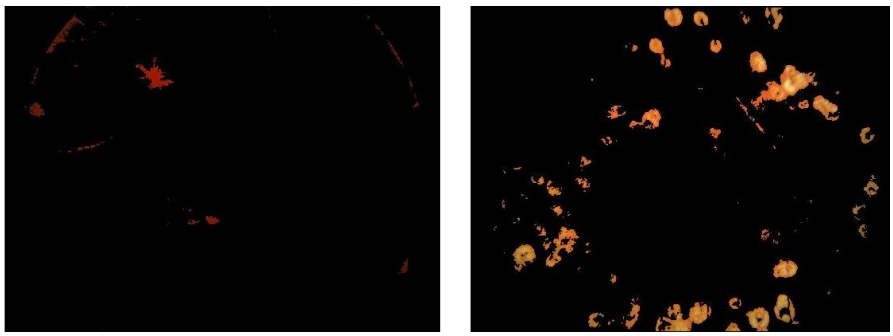

(a) (b)

Figure 36: Color images of segmented
(a) Dark lesions (b) Light lesions

Six features are extracted from each related region and the features are used for training and testing classifier. As explained in Section 3.3 these features are *area, mean gradient, mean hue, mean saturation, mean value and eccentricity*. These features are calculated as follows.

- Area: The number of pixels in a segmented region which is calculated using Matlab function 'area'.
- Mean gradient: For this feature, colored lesion images are converted to gray scale image firstly. For each region, gradient is calculated over non-zero pixels and averaged over all pixels in the region.
- Mean hue: Again we need the colored images but it should be converted from RGB into HSV format. After extracting hue (H channel), it is averages over all non-zero pixels of region.
- Mean saturation: Using S channel of HSV image, the mean value of saturation over all non-zero pixels is calculated for the segmented region.
- Mean value: This is also calculated using V channel of HSV image. Average value over all non-zero pixels in a region is computed.
- Eccentricity: This feature is a shape describer to measure circularity of the region. If an ellipse is fitted to the region, this is the ration of smaller diameter to the larger one. So the value of this feature varies between 0 (for a line object) to 1 (for a circular object) for each region.

A sample of feature matrix for dark lesions segmented in one of the images is shown in Figure 37. This example shows the un-normalized matrix of samples. As one can see, the scales are features are completely different. Before applying SVM, all samples

are normalized. In each fold, features are normalized using zero-mean unit variance method to compensate the differences in features' scales.

Area	mean hue	mean saturation	mean value	ecentricity	mean gradient
13	0.0499	0.9948	0.3427	0.7257	0.0024
710	0.0382	0.9501	0.4152	0.9935	0.0678
67	0.0385	0.9749	0.4601	0.9368	0.0130
18	0.0383	0.9947	0.4917	0.3435	0.0042
16	0.0383	0.9851	0.4801	0.9374	0.0045
13	0.0358	0.9882	0.5176	0.8312	0.0035
10	0.0478	0.9689	0.3784	0.9185	0.0027
11	0.0469	0.9871	0.3430	0.7689	0.0022
47	0.0440	0.9028	0.3414	0.9435	0.0081

Figure 37: A sample of feature matrix for dark lesions

4.5 Performance Measures

In this study, five performance metrics are calculated including ***accuracy, sensitivity,*** and ***specificity.*** After finishing all 5-folds, the mean value of these metrics is reported. In this work, metrics are computed based on two schemes: ***region-based*** and ***image-based***.

In ***pixel-based calculation*** the number of pixels in each segment is the unit for calculation, i.e. if a specific anomaly is detected correctly; all its pixels are contributed to accuracy. On the other hand, if an anomaly is not recognized correctly, all the pixels are considered. This way, a small wrongly detected segment cannot reduce the performance remarkably.

In ***segment-based scheme***, the unit of calculation for correctly detected or wrongly detected anomalies is region. The number of errorless regions for instance is divided by the total number of segmented regions to compute accuracy. And finally in image-based scheme, images are the unit of calculation. Abnormal and normal accuracy

values are computed using this scheme. In the following, the formula for each performance metric is represented.

$$\text{Accuracy} = \frac{\text{Number of correctly classified units}}{\text{Total number of units}} = \frac{T_P + T_N}{T_P + T_N + F_P + F_N} \quad (4)$$

where unit can be pixel, region or image. In Formula number 4, T_P, T_N, F_P and F_N are true positives, true negatives, false positives and false negatives respectively. These terms are explained in the following.

T_P is the number of positive samples which are labels as positive by the classification system. This is a measure of how system is sensible to positive cases.

T_N is the number of negative samples which are labels as negative by the classification system. In other words, it shows how system is specified to put negatives in negative class.

F_P is the number of negative samples which are labels as positive by the classification system. This value shows the error of system in detecting negative samples.

F_N is the number of positive samples which are labels as negative by the classification system. This value shows the error of system in detecting positive samples.

There are two other performance measures to evaluate system accuracy for normal and abnormal images separately. These metrics are called sensitivity (or abnormal accuracy) and specificity (or normal accuracy). The related formulas are as follows.

$$\text{Sensitivity} = \frac{\text{TP}}{\text{TP} + \text{FN}} \quad (5)$$

$$\text{Specificity} = \frac{\text{TN}}{\text{TN} + \text{FP}} \tag{6}$$

4.6 Comparisons with Other Approaches

In this area, different methods have been suggested and applied for automated segmentation of lesions in retinal images and for retinal disease detection as well. In order to summarize these methods in an understandable way, a more detailed table is prepared. The overall picture on the literature reviewed in this study, a summary table has been created in Table 5.

Table 5: Overview of the literarture and our proposed algorithm

Lesion/Disease type	**[14]**	**[17]**	**[18]**	**[21]**	**[22]**	**[24]**	**[25]**	**[26]**	**[27]**	**Ours**
OD	+	+	+	+	+	n/a	+	+	n/a	+
Blood Vessels	+	+	+	+	n/a	+	+	n/a	n/a	+
MA	+	+	+	n/a	n/a	n/a	n/a	n/a	n/a	+
H	+	n/a	+	n/a	n/a	n/a	n/a	n/a	n/a	+
NV	n/a	n/a	n/a	n/a	n/a	n/a	n/a	n/a	n/a	+
HE	+	+	+	+	n/a	n/a	+	+	n/a	+
CWS	+	n/a	+	n/a	n/a	n/a	n/a	+	n/a	+
Cataract/DR	n/a	n/a	n/a	n/a	n/a	n/a	n/a	n/a	+	n/a

In the first column of the table, lesions are listed including all lesion types found about fundus images. A plus '+' sign means that lesion have been considered in the investigated reference. A symbol 'n/a ' stands in the cases where the researchers have not mentioned about that lesion type or disease type.

In addition, available methodologies applied in different stages of fundus image processing are listed for this area. According to the investigated reference, a plus sign is put in the table. Using information in Table 5, one can easily understand the background of the problem and the architecture of the proposed algorithm compared to the reviewed literature.

Different methods using for each task in a DR detection system are listed in Table 6. Accordingly, it has been marked in each study which method is applied. This information makes it possible to compare already available methods with our proposed system architecture. In fact, a good selection of subsystems is the key point in designing a combined system for detecting all regions in fundus images. This is the strength of our study that all available segments are detected in retinal image unlike previous studies which mainly focused on specific region(s).

Table 6: Available methodologies for fundus image processing in literature

Steps	Methodology	[14]	[17]	[18]	[21]	[22]	[24]	[25]	[26]	[27]	Ours	Used Formula Method
Preprocessing	Median Filtering				+	+						
	Average Filtering			+				+		+	+	**Eq. 1**
	Noise Removal by Mask	+		+							+	**Alg. 1**
	Image Resizing		+		+							
	CLAHE Method		+									
	Contrast Adjustment		+			+				+		
	Gray and Green Channel		+									
	Morphological Operations			+								
	RGB to Gray Scale				+							
	Formatting/Segmentation								+			
Blood Vessels	Kirsch Method						+				+	**Alg. 3**
	Fuzzy C-Means		+									
	Morphological operations		+								+	
	2-D Gabor Wavelet			+								
	Thresholding			+							+	**Alg. 3**
	Histogram Thresholding				+							
	Smoothing				+							
OD	Histogram-based Template Matching					+					+	**Eq. 2** **Eq. 3**
	Optic Disk Mask		+								+	**Alg. 2**
	Canny Edge Detection		+									
	Average Filter			+						+		
	Hough Transform			+						+		
	Thresholding			+							+	**Alg. 2**
	Edge Detection			+								
	Sobel Edge Detection				+							
	Ellipse Fitting				+							
MA	Fuzzy Hybrid Neural Network			+								
	Morphological Operations		+							+		
	Feature Extraction	+									+	**Alg. 4**

	SVM										+	**SVMlight library, Eq. 4-8**
H	Fuzzy Hybrid Neural Network			+								
	Feature Extraction	+									+	**Alg. 4**
	SVM										+	**SVMlight library, Eq. 4-8**
NV	Thresholding											
	Feature Extraction							+			+	**Alg. 4**
	SVM										+	**SVMlight library, Eq. 4-8**
SE (CWS)	Feature Extraction	+								+	+	**Alg. 4**
	Fuzzy Hybrid Neural Network			+								
	Morphological Operations		+									
	K Nearest Neighbor				+							
	Neural Network							+				
	SVM										+	**SVMlight library, Eq. 4-8**
	GMM									+		
HE	Feature Extraction	+						+		+	+	**Alg. 4**
	Fuzzy Hybrid Neural Network			+								
	Morphological Operations		+									
	k Nearest Neighbor				+							
	Artificial Neural Network							+				
	SVM										+	**SVMlight library, Eq. 4-8**
										+		
Cataract/DR	Mobile Application								+			

Chapter 5

EXPERIMENTAL RESULTS

5.1 Experimental Setup

The main objective in this study is to implement a method for automatic detection of DR. Segmented regions are classified as anomalies for light and dark lesions separately. For classification, linear SVM is used. SVMlight binary library [29] is used for implementation of linear SVM. There are five types of anomalies labeled in the GT file including red small dots, H, HE, SE and NV. Red small dots, H and NV are segmented in dark lesions while the HE and CWS (or SE) are segmented in light lesions. In light lesions case, an SVM classifier is used which classifies the segments into the HE and CWS (or SE) categories. After classification, each image is assigned a tag of the detected anomalies. For dark lesions, there are three different segments. We firstly train a classifier which puts NV in class one and the two others (red small dots and H) in class two Since the NV has a linear shape compared to small dots and H are rounded. Therefore, there is a two level SVM classifier for dark lesions.

Experiments have been conducted on four data sets including DIARETDB0, DIARETDB1, STARE and HRF. In all the experiments, In order to split the data in train and test set, 5-fold cross validation is applied. In each fold, features are normalized using zero-mean unit variance method to compensate the differences in features' scales. Performance metrics are summed up amongst all folds.

The experiments have conducted on all four data sets. DIARETDB0 and DIARETDB1 data sets are used completely i.e. experiments are conducted on all images. For HRF data set, 15 images diagnosed with different disease are discarded and 30 images are used including 15 normal and 15 DR images. From STARE data set a subset of 40 images is selected including 20 normal and 20 DR images. All the experiments have repeated 5 times based on 5-fold cross validation. Since there are 130 images in the DIARETDB0 data set, in each fold we use 104 images for training and 26 images for testing SVM classifier. For DIARETDB1, there are 89 images hence there are 71 images in training set and 18 images in testing set in each fold. For HRF, train set contains 24 images and test set contains 6 images per fold. Lastly, for STARE subset, in each fold there are 32 and 8 images in train and test set respectively. Linear SVM is used and implemented at this point by SVMlight library as explained in previous chapter.

5.2 Experimental Results

After running the experiments, performance measures are recorded for each fold. The final reported results are the summation of them. Accuracy, sensitivity and specificity (as explained in Section 4.5) are calculated in three ways: *image based*, *region-based* and *grading-based*. The difference between these three calculation methods are: *image based* focuses only images, but *region-based* focuses on parts (such as MA, NV, H, SE and HE). The *grading-based* evaluation considers only assigned grading value by proposed system and compare it with the grade value inside GT file. In other word, the formulas are the same but according to the following descriptions, the units of measure differs.

— ***Image-based scheme:*** Image is the unit for counting performance numbers such as T_P, T_N, F_P, F_N. More precisely, if any abnormal region is detected in an image, it is labeled as positive, unless it is considered as a normal subject.

In Table 7, image based performance metrics are represented for all data sets. In the last row, total measures based on all data sets are reported. In order to make the results clear, all numbers including T_P, T_N, F_P, and F_N are written in the table. It can be argued that, system performance depends on the data set and sensitivity and specificity are changing according to the distribution of images in two classes (DR and normal). For DIARETDB1 for instance, as the number of normal images is very few (5 images), specificity is poor. The table gives the overall picture of the system performance on different data sets. The best accuracy result is obtained on DIARETDB1 and the poorest on DIARETDB0.

Table 7: Image-based perfromance measures for proposed system

Data set	T_P	T_N	F_P	F_N	Sensitivity	Specificity	Accuracy
DIARETDB0	91	14	6	19	82.73	70.00	80.77
DIARETDB1	76	3	2	8	90.48	60.00	88.76
STARE	56	51	7	11	83.58	87.93	85.60
HRF	12	14	1	3	80.00	93.34	86.67

Region-based scheme: Another perspective which may help evaluating the system performance is its efficiency in detecting exudates (both HE and SE) since these regions are critical in DR detection. In Table 8, exudate detection performance is reported for proposed method. When the region tag is matched with GT it is considered as a correctly classified document. The numbers are divided by total number of regions

in test images. All initial performance metrics (T_P, T_N, F_P, F_N) are computed by counting related regions. The results are compared with a study by Akram et al. [26] which focused on exudate detection for DR detection. According to the table, results are relatively comparable. In fact, proposed method surpasses the mentioned work for DIARETDB0 but the performance is slightly lower for DIARETDB1.

Table 8: Exudate detection perfromance (Region-based measures)

Method	Data set	T_P	T_N	F_P	F_N	Sensitivity	Specificity	Accuracy
Proposed	DIARETDB0	490	871	14	28	94.59	98.41	97.01
	DIARETDB1	386	413	8	2	99.48	97.64	98.76
Akram et. al	DIARETDB0	357	548	9	24	93.70	98.38	96.48
[26]	DIARETDB1	288	357	6	1	99.65	98.35	98.92

In order to compare our result with recent literature in the field on DR detection, a summary of some of them has been listed in Table 9. These studies worked on different data sets aiming at different tasks in DR detection. Comparisons are also confirmed that proposed system is reliable and generally superior to previous works. Used methods in these references are depicted in Table 6. In cases when results were reported individually for each data set, the details are written in the table. But in case of Akram and Khan [18], only overall accuracy was represented. From both perspectives, proposed algorithm is efficient when compare to others.

Grading-based scheme: The final experiment conducted in this study is grading. Grading DR for any fundus image is important for treatment of the disease. As mentioned in Chapter 1, there are 5 grades for DR including normal, mild, moderate, severe and PDR.

Table 9: Performance comparison in DR detection filed (region-based)

Method	Data set	#Images	Sensitivity	Specificity	Accuracy
Kuivalainen [14]	DIARETDB0	130	80.67	65	76.70
Harini & Sheela [17]	DIARETDB0/DIARETDB1	75	100	95.83	96.67
Akram & Khan [18]	DRIVE	40			
	STARE	81			
	DIARETDB0	130	-	-	93.71
	DIARETDB1	89			
Gowda et al [25]	DIARETDB1	10	96.97	100	98.45
Akram et. al [26]	STARE	n/a	97.72	96.15	95.56
	DIARETDB0	130	93.70	98.38	96.48
	DIARETDB1	89	98.65	98.35	98.92
Bourouis [27]	DIARETDB0/STARE	130/70	87.50	91.87	-
Proposed	**DIARETDB0**	**130**	**94.59**	**98.41**	**97.01**
	DIARETDB1	**89**	**99.48**	**97.64**	**98.76**

If an image does not contain any signs of anomaly, it will be considered as normal. For grading-based results evaluation, experiments are just conducted on DIARETDB0 data set which has more images compared to others and contains also a GT file. Based on Algorithm 5 explained in Chapter 3, an if-else architecture is applied on automatically segmented fundus images to grade them. The GT file of the DIARETDB0 with true detections is used as the reference (see Appendix A for the whole information). Finally, the graded images are compared with the grades obtained using GT document. The complete retrieved results for grading are represented in Appendix B. Overall accuracy is computed by comparing the result of automated grading with that of grading based on GT. It has been observed that out of 130 images in DIARETDB0 data set 96 images are graded correctly which means 73.85% accuracy in automated grading.

Chapter 6

CONCLUSION

Diabetic Retinopathy (DR) is a serious complication of diabetes that can result in severe conditions such as loss of vision and blindness. This study aimed at addressing the problem of automatic detection of DR. As the technology advances, more researchers are becoming interested in intelligent diagnosis systems to assist screening for specific diseases such as diabetes and its complications. DR is a common disease among patients with diabetes and it is vital to diagnose, treat and control it at early stage.

Colored retinal images are recorded for diagnosis of DR. Medical experts diagnose DR from specific dark and light lesions in colored fundus images. There are different segments possibly appearing in fundus images including OD, blood vessels, dark lesions (Microaneurysm (MA), Hemorrhage (H) and Neuvascularization (NV)), and light lesions (Hard Exudates (HE) and Soft Exudates (SE) or Cotton Wool Spots (CWS)). Detection and severity level of DR depends on the existence of these lesions in fundus images and the degree of them.

In this thesis, a fully automated system is proposed for automatic detection of lesions and accordingly grading DR. The proposed system is implemented as follows. After removing noisy area, Optical Disk (OD) is located in images based on a histogram template method. Then, using thresholding a black and white mask is produced to

remove optical disk from fundus images. The network of blood vessels need also to be removed. Based on Kirsch edge enhancement technique, blood vessels are masked. The next step of segmentation is searching for dark and light lesions. In the next phase, six features related to anatomical characteristics of anomalies in retinal images are extracted. These features are related to size, shape, color and brightness of the regions. Support Vector Machine (SVM) classifier is the last block of the system. Light lesions and dark lesions are separately classified into their corresponding anomalies using linear SVM classifier.

In the last stage, 5-fold cross validation is used to avoid bias in selection of train and test sets. Totally, our experiments are conducted on four data sets including DIARETDB0, DIARETDB1, HRF and STARE. The results have proved that accuracy, sensitivity, and specificity of the proposed system are all comparable or superior to several state-of-the-art methods.

For better comparison, exudate detection performance is also reported and compared to recent studies. In the last step, based on the detected abnormal lesions, the degree of severity of DR is automatically defined. Experimental results have shown that images are graded with an acceptable accuracy compared to GT documents. It can be concluded that for all four data sets, system performance in DR detection and grading is acceptable.

The experimental setting of this study is based on the most recently published papers in this field. Our results are sensibly comparable to other studies. The main weakness of this work however, is the lack of a complete data set with a more precise GT. In the

future, a better grading system that matches more with medical definition can be designed using such a data set.

REFERENCES

[1] Diabetic Retinopathy: What You Should Know, U.S. Department Of Health And Human Services, National Institutes of Health, National Eye Institute (2017, July 5), Retrieved from https://nei.nih.gov/sites/default/files/Diabetic-Retinopathy-What-You-Should-Know-508.pdf

[2] Pre-proliferative /non-proliferative retinopathy. Diabeticretinopathy.org.uk. (2017, July 5), Retrieved from http://www.diabeticretinopathy.org.uk/pre-proliferative.html

[3] Diabetic Retinopathy and Diabetic Macular Edema in Review. Zélia M. da Silva C. (2017, July 11), Retrieved from http://www.caringfordiabetes.com/ContinuingEducation/DiabeticMicroComplicationsActivities/Foresight/Activity/wocenewsletterpreso1.htm

[4] Klein, R. (1999). Editorial: Guidelines for screening for diabetic retinopathy revisited. Ophthalmic Epidemiology, 6(1), 1-4. doi: 10.1076/opep.6.1.1.1568

[5] Diabetic Retinopathy. (2002). Diabetes Care, 25(Supplement 1), S90-S93. doi: 10.2337/diacare.25.2007.s90

[6] Neely, K., Quillen, D., Schachat, A., Gardner, T., & Blankenship, G. (1998). Diabetic Retinopathy. Medical Clinics Of North America, 82(4), 847-876. doi: 10.1016/s0025-7125(05)70027-4

[7] Diabetic Retinopathy, (2017, July 25), Retrieved from http://wjscottmd.com /diabetic-retinopathy/

[8] Proliferative Diabetic Retinopathy (PDR), (2017, July 25), Retrieved from http://www.newhealthguide.org/Pdr.html

[9] Li, H., & Chutatape, O. Fundus image features extraction. Proceedings Of The 22Nd Annual International Conference Of The IEEE Engineering In Medicine And Biology Society (Cat. No.00CH37143). doi: 10.1109/iembs.2000.901530

[10] Kauppi, T., Kalesnykiene, V., Kamarainen, J.-K., Lensu, L., Sorri, I., Uusitalo, H., Kälviäinen, H., Pietilä, J., (2006). DIARETDB0: Evaluation Database and Methodology for Diabetic Retinopathy Algorithms, Technical report.

[11] Kauppi, T., Kalesnykiene, V., Kamarainen, J.-K., Lensu, L., Sorri, I., Raninen A., Voutilainen R., Uusitalo, H., Kälviäinen, H., Pietilä, J., (2007). DIARETDB1 diabetic retinopathy database and evaluation protocol, Technical report.

[12] Hoover, A., Kouznetsova V., and Goldbaum, M., (2000). Locating Blood Vessels in Retinal Images by Piece-wise Threhsold Probing of a Matched Filter Response, IEEE Transactions on Medical Imaging , 19(3), 203-210.

[13] Odstrcilik, J., Kolar, R., Kubena, T., Cernosek, P., Budai, A., & Hornegger, J. et al. (2013). Retinal vessel segmentation by improved matched filtering: evaluation on a new high-resolution fundus image database. IET Image Processing, 7(4), 373-383. doi: 10.1049/iet-ipr.2012.0455.

[14] Kuivalainen, M.. (2005) Retinal image analysis using machine vision.Master's thesis, Lappeenranta University of technology, 2005, Finland.

[15] Pratt, W. (2014). Introduction to digital image processing. Boca Raton [Fla.]: CRC Press, Taylor & Francis Group.

[16] Gander, W., Golub, G., & Strebel, R. (1994). Least-squares fitting of circles and ellipses. BIT, 34(4), 558-578. doi: 10.1007/bf01934268

[17] Harini R, & Sheela N. (2016). Feature extraction and classification of retinal images for automated detection of Diabetic Retinopathy. 2016 Second International Conference On Cognitive Computing And Information Processing (CCIP). doi: 10.1109/ccip.2016.7802862

[18] Akram, U., & Khan, S. (2011). Automated Detection of Dark and Bright Lesions in Retinal Images for Early Detection of Diabetic Retinopathy. Journal Of Medical Systems, 36(5), 3151-3162. doi:10.1007/s10916-011-9802-2

[19] Sekhar, S., Al-Nuaimy, W., & K. Nandi, A. (2008). Automated localisation of retinal optic disk using Hough transform. 2008 5Th IEEE International Symposium On Biomedical Imaging: From Nano To Macro. doi: 10.1109/isbi.2008.4541312

[20] Chapter I: DRUSEN OF THE OPTIC DISK. (2009). Acta Ophthalmologica, 44(S90), 9-21. doi: 10.1111/j.1755-3768.1966.tb06454.x

[21] Argade, K., Deshmukh, K., Narkhede, M., Sonawane, N., & Jore, S. (2015). Automatic detection of diabetic retinopathy using image processing and data mining techniques. 2015 International Conference On Green Computing And Internet Of Things (Icgciot). doi:10.1109/icgciot.2015.7380519

[22] Wankhede, P., & Khanchandani, K. (2016). Optic disc detection using histogram based template matching. 2016 International Conference On Signal Processing, Communication, Power And Embedded System (SCOPES). doi: 10.1109/scopes.2016.7955765

[23] Kirsch, R. (1971). Computer determination of the constituent structure of biological images. Computers And Biomedical Research, 4(3), 315-328. doi: 10.1016/0010-4809(71)90034-6

[24] H.S. Bhadauria, H. (2013). Vessels Extraction from Retinal Images. IOSR Journal Of Electronics And Communication Engineering, 6(3), 79-82. http://dx.doi.org/10.9790/2834-0637982

[25] Gowda, A., Nasiha, A., Jayaram, M., & . Manjunath, A. (2011). Exudates Detection in Retinal Images using Back Propagation Neural Network. International Journal Of Computer Applications, 25(3), 25-31. doi: 10.5120/3011-4062

[26] Akram, M., Tariq, A., Anjum, M., & Javed, M. (2012). Automated detection of exudates in colored retinal images for diagnosis of diabetic retinopathy. Applied Optics, 51(20), 4858. http://dx.doi.org/10.1364/ao.51.004858

[27] Bourouis, A., Feham, M., Hossain, M., & Zhang, L. (2014). An intelligent mobile based decision support system for retinal disease diagnosis. Decision Support Systems, 59, 341-350. doi: 10.1016/j.dss.2014.01.005

[28] Otsu, N. (1979). A Threshold Selection Method from Gray-Level Histograms. IEEE Transactions On Systems, Man, And Cybernetics, 9(1), 62-66. doi: 10.1109/tsmc.1979.4310076

[29] Joachims, T. (1999). Making large-Scale SVM Learning Practical. Advances in Kernel Methods - Support Vector Learning, B. Schölkopf and C. Burges and A. Smola (ed.), MIT-Press.

[30] Vapnik, N. (1995). The Nature of Statistical Learning Theory. Springer.

[31] Learning to Classify Text Using Support Vector Machines. (19 September 2017) Retrieved from http://Thorsten Joachims, Learning to Classify Text Using Support Vector Machines. Dissertation, Kluwer, 2002.

[32] Shanthi, R., and S. Prabakaran. "Fundus Abnormalities and Image Acquisition Techniques–A Survey."

[33] Xiong, Li, Huiqi Li, and Liang Xu. "An Approach to Evaluate Blurriness in Retinal Images with Vitreous Opacity for Cataract Diagnosis." Journal of Healthcare Engineering 2017 (2017).

[34] Schlanitz, Ferdinand G., et al. "Identification of drusen characteristics in age-related macular degeneration by polarization-sensitive optical coherence mography." *American journal of ophthalmology* 160.2 (2015): 335-344.

APPENDICES

Appendix A: GT (GT) file

IMG ID	FIVE CONSIDERED ANOMALY TYPES FOUND					RESULT GRADE
1	'redsmalldots'	'hemorrhages'	'hardexudates'	'n/a'	'n/a'	'severe'
2	'redsmalldots'	'hemorrhages'	'hardexudates'	'n/a'	'n/a'	'severe'
3	'redsmalldots'	'hemorrhages'	'hardexudates'	'softexudates'	'n/a'	'severe'
4	'redsmalldots'	'hemorrhages'	'hardexudates'	'n/a'	'n/a'	'severe'
5	'redsmalldots'	'hemorrhages'	'hardexudates'	'softexudates'	'n/a'	'severe'
6	'redsmalldots'	'hemorrhages'	'hardexudates'	'n/a'	'n/a'	'severe'
7	'redsmalldots'	'hemorrhages'	'hardexudates'	'n/a'	'n/a'	'severe'
8	'redsmalldots'	'hemorrhages'	'hardexudates'	'n/a'	'n/a'	'severe'
9	'redsmalldots'	'hemorrhages'	'hardexudates'	'softexudates'	'n/a'	'severe'
10	'redsmalldots'	'hemorrhages'	'hardexudates'	'softexudates'	'n/a'	'severe'
11	'redsmalldots'	'hemorrhages'	'hardexudates'	'softexudates'	'n/a'	'severe'
12	'redsmalldots'	'hemorrhages'	'hardexudates'	'n/a'	'n/a'	'severe'
13	'redsmalldots'	'hemorrhages'	'hardexudates'	'n/a'	'n/a'	'severe'
14	'redsmalldots'	'hemorrhages'	'hardexudates'	'softexudates'	'n/a'	'severe'
15	'redsmalldots'	'hemorrhages'	'hardexudates'	'n/a'	'n/a'	'severe'
16	'redsmalldots'	'hemorrhages'	'hardexudates'	'n/a'	'n/a'	'severe'
17	'redsmalldots'	'hemorrhages'	'hardexudates'	'n/a'	'n/a'	'severe'
18	'redsmalldots'	'hemorrhages'	'hardexudates'	'n/a'	'n/a'	'severe'
19	'redsmalldots'	'hemorrhages'	'hardexudates'	'n/a'	'n/a'	'severe'
20	'n/a'	'n/a'	'hardexudates'	'n/a'	'n/a'	'severe'
21	'redsmalldots'	'hemorrhages'	'hardexudates'	'n/a'	'n/a'	'severe'
22	'redsmalldots'	'hemorrhages'	'hardexudates'	'n/a'	'n/a'	'severe'
23	'redsmalldots'	'hemorrhages'	'hardexudates'	'n/a'	'n/a'	'severe'
24	'redsmalldots'	'hemorrhages'	'hardexudates'	'n/a'	'n/a'	'severe'
25	'redsmalldots'	'hemorrhages'	'hardexudates'	'softexudates'	'n/a'	'severe'
26	'redsmalldots'	'hemorrhages'	'hardexudates'	'softexudates'	'n/a'	'severe'
27	'redsmalldots'	'hemorrhages'	'hardexudates'	'softexudates'	'n/a'	'severe'
28	'redsmalldots'	'hemorrhages'	'hardexudates'	'n/a'	'n/a'	'severe'
29	'redsmalldots'	'hemorrhages'	'hardexudates'	'n/a'	'n/a'	'severe'
30	'redsmalldots'	'hemorrhages'	'hardexudates'	'n/a'	'n/a'	'severe'
31	'redsmalldots'	'hemorrhages'	'hardexudates'	'softexudates'	'neovascularisation'	'PDR'
32	'redsmalldots'	'hemorrhages'	'hardexudates'	'softexudates'	'neovascularisation'	'PDR'
33	'redsmalldots'	'hemorrhages'	'hardexudates'	'n/a'	'neovascularisation'	'PDR'
34	'redsmalldots'	'hemorrhages'	'hardexudates'	'n/a'	'neovascularisation'	'PDR'
35	'redsmalldots'	'hemorrhages'	'hardexudates'	'n/a'	'neovascularisation'	'PDR'
36	'redsmalldots'	'hemorrhages'	'n/a'	'softexudates'	'neovascularisation'	'PDR'
37	'redsmalldots'	'hemorrhages'	'n/a'	'softexudates'	'neovascularisation'	'PDR'
38	'redsmalldots'	'hemorrhages'	'n/a'	'softexudates'	'neovascularisation'	'PDR'
39	'redsmalldots'	'hemorrhages'	'n/a'	'softexudates'	'neovascularisation'	'PDR'
40	'redsmalldots'	'hemorrhages'	'n/a'	'n/a'	'neovascularisation'	'PDR'
41	'redsmalldots'	'hemorrhages'	'hardexudates'	'n/a'	'neovascularisation'	'PDR'
42	'redsmalldots'	'hemorrhages'	'n/a'	'n/a'	'neovascularisation'	'PDR'
43	'redsmalldots'	'hemorrhages'	'hardexudates'	'softexudates'	'neovascularisation'	'PDR'
44	'redsmalldots'	'hemorrhages'	'hardexudates'	'softexudates'	'neovascularisation'	'PDR'
45	'redsmalldots'	'hemorrhages'	'n/a'	'softexudates'	'neovascularisation'	'PDR'
46	'redsmalldots'	'hemorrhages'	'hardexudates'	'softexudates'	'neovascularisation'	'PDR'
47	'redsmalldots'	'hemorrhages'	'hardexudates'	'n/a'	'neovascularisation'	'PDR'
48	'redsmalldots'	'hemorrhages'	'hardexudates'	'n/a'	'neovascularisation'	'PDR'
49	'redsmalldots'	'hemorrhages'	'n/a'	'n/a'	'neovascularisation'	'PDR'
50	'n/a'	'n/a'	'n/a'	'n/a'	'Neovascularisation'	'PDR'
51	'redsmalldots'	'hemorrhages'	'hardexudates'	'softexudates'	'n/a'	'severe'
52	'redsmalldots'	'hemorrhages'	'hardexudates'	'softexudates'	'n/a'	'severe'
53	'redsmalldots'	'n/a'	'hardexudates'	'n/a'	'n/a'	'severe'
54	'redsmalldots'	'n/a'	'hardexudates'	'n/a'	'n/a'	'severe'
55	'redsmalldots'	'hemorrhages'	'hardexudates'	'n/a'	'n/a'	'severe'
56	'redsmalldots'	'n/a'	'hardexudates'	'n/a'	'n/a'	'severe'
57	**'redsmalldots'**	**'hemorrhages'**	**'n/a'**	**'softexudates'**	**'n/a'**	**'severe'**
58	'redsmalldots'	'n/a'	'n/a'	'softexudates'	'n/a'	'severe'

59	'redsmalldots'	'n/a'	'hardexudates'	'n/a'	'n/a'	'severe'
60	'redsmalldots'	'n/a'	'n/a'	'n/a'	'n/a'	'mild'
61	'redsmalldots'	'n/a'	'n/a'	'n/a'	'n/a'	'mild'
62	'redsmalldots'	'n/a'	'n/a'	'n/a'	'n/a'	'mild'
63	'redsmalldots'	'n/a'	'n/a'	'n/a'	'n/a'	'mild'
64	'redsmalldots'	'n/a'	'n/a'	'n/a'	'n/a'	'mild'
65	'redsmalldots'	'n/a'	'hardexudates'	'n/a'	'n/a'	'severe'
66	'redsmalldots'	'hemorrhages'	'hardexudates'	'n/a'	'n/a'	'severe'
67	'redsmalldots'	'n/a'	'n/a'	'n/a'	'n/a'	'mild'
68	'redsmalldots'	'n/a'	'n/a'	'n/a'	'n/a'	'mild'
69	'redsmalldots'	'hemorrhages'	'hardexudates'	'n/a'	'n/a'	'severe'
70	'redsmalldots'	'hemorrhages'	'n/a'	'n/a'	'n/a'	'moderate'
71	'redsmalldots'	'hemorrhages'	'hardexudates'	'softexudates'	'n/a'	'severe'
72	'redsmalldots'	'hemorrhages'	'hardexudates'	'softexudates'	'n/a'	'severe'
73	'redsmalldots'	'hemorrhages'	'n/a'	'softexudates'	'n/a'	'severe'
74	'redsmalldots'	'hemorrhages'	'hardexudates'	'softexudates'	'n/a'	'severe'
75	'redsmalldots'	'hemorrhages'	'n/a'	'n/a'	'n/a'	'moderate'
76	'redsmalldots'	'hemorrhages'	'n/a'	'n/a'	'n/a'	'moderate'
77	'redsmalldots'	'hemorrhages'	'hardexudates'	'softexudates'	'n/a'	'severe'
78	'redsmalldots'	'hemorrhages'	'hardexudates'	'softexudates'	'n/a'	'severe'
79	'redsmalldots'	'hemorrhages'	'hardexudates'	'n/a'	'n/a'	'severe'
80	'redsmalldots'	'hemorrhages'	'n/a'	'n/a'	'n/a'	'moderate'
81	'redsmalldots'	'hemorrhages'	'n/a'	'n/a'	'n/a'	'moderate'
82	'n/a'	'n/a'	'n/a'	'n/a'	'n/a'	'normal'
83	'redsmalldots'	'hemorrhages'	'hardexudates'	'n/a'	'n/a'	'severe'
84	'redsmalldots'	'hemorrhages'	'n/a'	'softexudates'	'n/a'	'severe'
85	'redsmalldots'	'n/a'	'n/a'	'n/a'	'n/a'	'mild'
86	'redsmalldots'	'n/a'	'n/a'	'n/a'	'n/a'	'mild'
87	'redsmalldots'	'n/a'	'n/a'	'n/a'	'n/a'	'mild'
88	'redsmalldots'	'n/a'	'n/a'	'n/a'	'n/a'	'mild'
89	'redsmalldots'	'n/a'	'n/a'	'n/a'	'n/a'	'mild'
90	'redsmalldots'	'n/a'	'n/a'	'n/a'	'n/a'	'mild'
91	'redsmalldots'	'n/a'	'n/a'	'n/a'	'n/a'	'mild'
92	'redsmalldots'	'n/a'	'n/a'	'softexudates'	'n/a'	'severe'
93	'redsmalldots'	'hemorrhages'	'hardexudates'	'n/a'	'n/a'	'severe'
94	'redsmalldots'	'n/a'	'n/a'	'n/a'	'n/a'	'mild'
95	'n/a'	'n/a'	'n/a'	'n/a'	'n/a'	'normal'
96	'redsmalldots'	'n/a'	'hardexudates'	'n/a'	'n/a'	'severe'
97	'redsmalldots'	'n/a'	'n/a'	'n/a'	'n/a'	'mild'
98	'redsmalldots'	'n/a'	'n/a'	'softexudates'	'n/a'	'severe'
99	'redsmalldots'	'n/a'	'n/a'	'n/a'	'n/a'	'mild'
100	'redsmalldots'	'hemorrhages'	'hardexudates'	'softexudates'	'n/a'	'severe'
101	'redsmalldots'	'hemorrhages'	'hardexudates'	'softexudates'	'n/a'	'severe'
102	'redsmalldots'	'hemorrhages'	'hardexudates'	'softexudates'	'n/a'	'severe'
103	'redsmalldots'	'hemorrhages'	'hardexudates'	'softexudates'	'n/a'	'severe'
104	'redsmalldots'	'hemorrhages'	'hardexudates'	'n/a'	'n/a'	'severe'
105	'redsmalldots'	'hemorrhages'	'hardexudates'	'n/a'	'n/a'	'severe'
106	'redsmalldots'	'hemorrhages'	'hardexudates'	'softexudates'	'n/a'	'severe'
107	'redsmalldots'	'hemorrhages'	'hardexudates'	'softexudates'	'n/a'	'severe'
108	'redsmalldots'	'hemorrhages'	'hardexudates'	'softexudates'	'n/a'	'severe'
109	'redsmalldots'	'hemorrhages'	'hardexudates'	'softexudates'	'n/a'	'severe'
110	'redsmalldots'	'hemorrhages'	'hardexudates'	'softexudates'	'n/a'	'severe'
111	'n/a'	'n/a'	'n/a'	'n/a'	'n/a'	'normal'
112	'n/a'	'n/a'	'n/a'	'n/a'	'n/a'	'normal'
113	'n/a'	'n/a'	'n/a'	'n/a'	'n/a'	'normal'
114	'n/a'	'n/a'	'n/a'	'n/a'	'n/a'	'normal'
115	'n/a'	'n/a'	'n/a'	'n/a'	'n/a'	'normal'
116	'n/a'	'n/a'	'n/a'	'n/a'	'n/a'	'normal'
117	'n/a'	'n/a'	'n/a'	'n/a'	'n/a'	'normal'
118	'n/a'	'n/a'	'n/a'	'n/a'	'n/a'	'normal'
119	'n/a'	'n/a'	'n/a'	'n/a'	'n/a'	'normal'
120	'n/a'	'n/a'	'n/a'	'n/a'	'n/a'	'normal'
121	'n/a'	'n/a'	'n/a'	'n/a'	'n/a'	'normal'
122	'n/a'	'n/a'	'n/a'	'n/a'	'n/a'	'normal'
123	'n/a'	'n/a'	'n/a'	'n/a'	'n/a'	'normal'

124	'n/a'	'n/a'	'n/a'	'n/a'	'n/a'	'normal'
125	'n/a'	'n/a'	'n/a'	'n/a'	'n/a'	'normal'
126	'n/a'	'n/a'	'n/a'	'n/a'	'n/a'	'normal'
127	'n/a'	'n/a'	'n/a'	'n/a'	'n/a'	'normal'
128	'n/a'	'n/a'	'n/a'	'n/a'	'n/a'	'normal'
129	'n/a'	'n/a'	'n/a'	'n/a'	'n/a'	'normal'
130	'n/a'	'n/a'	'n/a'	'n/a'	'n/a'	'normal'

Appendix B: Predicted Abnormal Lesions

IMG ID	FIVE CONSIDERED ANOMALY TYPES FOUND					RESULT GRADE
1	'redsmalldots'	'hemorrhages'	'hardexudates'	'n/a'	'n/a'	'severe'
2	'redsmalldots'	'hemorrhages'	'hardexudates'	'n/a'	'n/a'	'severe'
3	'n/a'	'n/a'	'hardexudates'	'softexudates'	'n/a'	'severe'
4	'redsmalldots'	'hemorrhages'	'n/a'	'n/a'	'n/a'	'moderate'
5	'redsmalldots'	'n/a'	'n/a'	'n/a'	'n/a'	'mild'
6	'redsmalldots'	'hemorrhages'	'n/a'	'n/a'	'n/a'	'moderate'
7	'redsmalldots'	'hemorrhages'	'hardexudates'	'softexudates'	'n/a'	'severe'
8	'redsmalldots'	'hemorrhages'	'hardexudates'	'n/a'	'n/a'	'severe'
9	'redsmalldots'	'hemorrhages'	'hardexudates'	'softexudates'	'n/a'	'severe'
10	'n/a'	'hemorrhages'	'n/a'	'softexudates'	'n/a'	'severe'
11	'redsmalldots'	'hemorrhages'	'hardexudates'	'softexudates'	'neovascularisation'	'PDR'
12	'redsmalldots'	'hemorrhages'	'n/a'	'n/a'	'n/a'	'moderate'
13	'redsmalldots'	'hemorrhages'	'hardexudates'	'n/a'	'n/a'	'severe'
14	'redsmalldots'	'hemorrhages'	'hardexudates'	'softexudates'	'n/a'	'severe'
15	'redsmalldots'	'hemorrhages'	'hardexudates'	'n/a'	'n/a'	'severe'
16	'redsmalldots'	'hemorrhages'	'hardexudates'	'n/a'	'neovascularisation'	'PDR'
17	'redsmalldots'	'hemorrhages'	'hardexudates'	'n/a'	'n/a'	'severe'
18	'redsmalldots'	'hemorrhages'	'hardexudates'	'n/a'	'n/a'	'severe'
19	'n/a'	'n/a'	'hardexudates'	'n/a'	'n/a'	'severe'
20	'n/a'	'n/a'	'hardexudates'	'n/a'	'n/a'	'severe'
21	'redsmalldots'	'hemorrhages'	'hardexudates'	'n/a'	'n/a'	'severe'
22	'redsmalldots'	'hemorrhages'	'hardexudates'	'n/a'	'n/a'	'severe'
23	'redsmalldots'	'hemorrhages'	'hardexudates'	'n/a'	'n/a'	'severe'
24	'redsmalldots'	'hemorrhages'	'hardexudates'	'n/a'	'n/a'	'severe'
25	'n/a'	'n/a'	'hardexudates'	'n/a'	'n/a'	'severe'
26	'redsmalldots'	'hemorrhages'	'hardexudates'	'softexudates'	'neovascularisation'	'PDR'
27	'redsmalldots'	'hemorrhages'	'hardexudates'	'softexudates'	'neovascularisation'	'PDR'
28	'redsmalldots'	'hemorrhages'	'hardexudates'	'n/a'	'neovascularisation'	'PDR'
29	'redsmalldots'	'hemorrhages'	'n/a'	'n/a'	'n/a'	'moderate'
30	'n/a'	'n/a'	'hardexudates'	'n/a'	'n/a'	'severe'
31	'redsmalldots'	'n/a'	'hardexudates'	'softexudates'	'n/a'	'severe'
32	'redsmalldots'	'hemorrhages'	'n/a'	'n/a'	'neovascularisation'	'PDR'
33	'redsmalldots'	'hemorrhages'	'n/a'	'n/a'	'n/a'	'moderate'
34	'redsmalldots'	'hemorrhages'	'hardexudates'	'n/a'	'neovascularisation'	'PDR'
35	'redsmalldots'	'hemorrhages'	'hardexudates'	'softexudates'	'neovascularisation'	'PDR'
36	'redsmalldots'	'hemorrhages'	'n/a'	'softexudates'	'n/a'	'severe'
37	'redsmalldots'	'hemorrhages'	'n/a'	'softexudates'	'neovascularisation'	'PDR'
38	'redsmalldots'	'hemorrhages'	'n/a'	'softexudates'	'neovascularisation'	'PDR'
39	'redsmalldots'	'hemorrhages'	'n/a'	'softexudates'	'n/a'	'severe'
40	'redsmalldots'	'hemorrhages'	'n/a'	'softexudates'	'neovascularisation'	'PDR'
41	'redsmalldots'	'hemorrhages'	'hardexudates'	'n/a'	'neovascularisation'	'PDR'
42	'redsmalldots'	'hemorrhages'	'hardexudates'	'softexudates'	'n/a'	'severe'
43	'redsmalldots'	'hemorrhages'	'hardexudates'	'softexudates'	'neovascularisation'	'PDR'
44	'redsmalldots'	'hemorrhages'	'hardexudates'	'softexudates'	'neovascularisation'	'PDR'
45	'redsmalldots'	'hemorrhages'	'n/a'	'softexudates'	'neovascularisation'	'PDR'
46	'redsmalldots'	'hemorrhages'	'hardexudates'	'n/a'	'neovascularisation'	'PDR'
47	'redsmalldots'	'hemorrhages'	'hardexudates'	'n/a'	'neovascularisation'	'PDR'
48	'redsmalldots'	'hemorrhages'	'n/a'	'n/a'	'neovascularisation'	'PDR'
49	'redsmalldots'	'hemorrhages'	'n/a'	'n/a'	'neovascularisation'	'PDR'
50	'n/a'	'hemorrhages'	'n/a'	'softexudates'	'neovascularisation'	'PDR'
51	'redsmalldots'	'hemorrhages'	'hardexudates'	'softexudates'	'n/a'	'severe'
52	'redsmalldots'	'hemorrhages'	'hardexudates'	'n/a'	'n/a'	'severe'
53	'redsmalldots'	'n/a'	'n/a'	'n/a'	'n/a'	'mild'
54	'redsmalldots'	'hemorrhages'	'n/a'	'n/a'	'n/a'	'moderate'
55	'redsmalldots'	'n/a'	'n/a'	'n/a'	'n/a'	'mild'
56	'n/a'	'n/a'	'n/a'	'n/a'	'n/a'	'normal'
57	'redsmalldots'	'n/a'	'n/a'	'n/a'	'neovascularisation'	'PDR'
58	'redsmalldots'	'hemorrhages'	'n/a'	'n/a'	'n/a'	'moderate'
59	'redsmalldots'	'n/a'	'n/a'	'n/a'	'n/a'	'mild'
60	'redsmalldots'	'n/a'	'hardexudates'	'n/a'	'n/a'	'severe'

61	'redsmalldots'	'n/a'	'n/a'	'n/a'	'n/a'	'mild'
62	'redsmalldots'	'n/a'	'n/a'	'n/a'	'n/a'	'mild'
63	'redsmalldots'	'n/a'	'n/a'	'n/a'	'n/a'	'mild'
64	'redsmalldots'	'n/a'	'n/a'	'n/a'	'n/a'	'mild'
65	'redsmalldots'	'n/a'	'hardexudates'	'n/a'	'n/a'	'severe'
66	'redsmalldots'	'hemorrhages'	'hardexudates'	'n/a'	'n/a'	'severe'
67	'redsmalldots'	'n/a'	'n/a'	'n/a'	'n/a'	'mild'
68	'redsmalldots'	'n/a'	'n/a'	'n/a'	'n/a'	'mild'
69	'redsmalldots'	'hemorrhages'	'hardexudates'	'n/a'	'n/a'	'severe'
70	'redsmalldots'	'hemorrhages'	'n/a'	'n/a'	'n/a'	'moderate'
71	'redsmalldots'	'hemorrhages'	'hardexudates'	'softexudates'	'n/a'	'severe'
72	'redsmalldots'	'hemorrhages'	'hardexudates'	'softexudates'	'n/a'	'severe'
73	'redsmalldots'	'n/a'	'n/a'	'softexudates'	'n/a'	'severe'
74	'n/a'	'hemorrhages'	'hardexudates'	'softexudates'	'n/a'	'severe'
75	'redsmalldots'	'hemorrhages'	'n/a'	'n/a'	'n/a'	'moderate'
76	'redsmalldots'	'hemorrhages'	'n/a'	'n/a'	'n/a'	'moderate'
77	'n/a'	'n/a'	'hardexudates'	'softexudates'	'n/a'	'severe'
78	'n/a'	'hemorrhages'	'hardexudates'	'softexudates'	'n/a'	'severe'
79	'redsmalldots'	'hemorrhages'	'hardexudates'	'n/a'	'n/a'	'severe'
80	'redsmalldots'	'hemorrhages'	'n/a'	'n/a'	'neovascularisation'	'PDR'
81	'redsmalldots'	'hemorrhages'	'n/a'	'n/a'	'n/a'	'moderate'
82	'n/a'	'n/a'	'n/a'	'n/a'	'n/a'	'normal'
83	'redsmalldots'	'hemorrhages'	'hardexudates'	'n/a'	'n/a'	'severe'
84	'redsmalldots'	'hemorrhages'	'n/a'	'softexudates'	'n/a'	'severe'
85	'n/a'	'n/a'	'n/a'	'n/a'	'n/a'	'normal'
86	'n/a'	'n/a'	'n/a'	'n/a'	'n/a'	'normal'
87	'redsmalldots'	'n/a'	'hardexudates'	'n/a'	'n/a'	'severe'
88	'redsmalldots'	'n/a'	'n/a'	'n/a'	'n/a'	'mild'
89	'redsmalldots'	'n/a'	'n/a'	'n/a'	'n/a'	'mild'
90	'redsmalldots'	'hemorrhages'	'n/a'	'n/a'	'n/a'	'moderate'
91	'redsmalldots'	'n/a'	'n/a'	'n/a'	'n/a'	'mild'
92	'redsmalldots'	'n/a'	'n/a'	'softexudates'	'n/a'	'severe'
93	'redsmalldots'	'hemorrhages'	'hardexudates'	'n/a'	'n/a'	'severe'
94	'redsmalldots'	'n/a'	'n/a'	'n/a'	'n/a'	'mild'
95	'redsmalldots'	'hemorrhages'	'n/a'	'softexudates'	'neovascularisation'	'PDR'
96	'redsmalldots'	'n/a'	'hardexudates'	'n/a'	'n/a'	'severe'
97	'redsmalldots'	'n/a'	'n/a'	'n/a'	'n/a'	'mild'
98	'redsmalldots'	'n/a'	'n/a'	'softexudates'	'n/a'	'severe'
99	'redsmalldots'	'n/a'	'n/a'	'n/a'	'n/a'	'mild'
100	'redsmalldots'	'hemorrhages'	'hardexudates'	'n/a'	'n/a'	'severe'
101	'redsmalldots'	'hemorrhages'	'n/a'	'softexudates'	'n/a'	'severe'
102	'redsmalldots'	'hemorrhages'	'hardexudates'	'softexudates'	'n/a'	'severe'
103	'redsmalldots'	'hemorrhages'	'hardexudates'	'softexudates'	'n/a'	'severe'
104	'redsmalldots'	'hemorrhages'	'hardexudates'	'softexudates'	'neovascularisation'	'PDR'
105	'redsmalldots'	'hemorrhages'	'hardexudates'	'n/a'	'n/a'	'severe'
106	'redsmalldots'	'hemorrhages'	'hardexudates'	'softexudates'	'n/a'	'severe'
107	'redsmalldots'	'hemorrhages'	'hardexudates'	'softexudates'	'n/a'	'severe'
108	'redsmalldots'	'hemorrhages'	'n/a'	'softexudates'	'n/a'	'severe'
109	'redsmalldots'	'hemorrhages'	'hardexudates'	'softexudates'	'n/a'	'severe'
110	'redsmalldots'	'hemorrhages'	'hardexudates'	'softexudates'	'n/a'	'severe'
111	'n/a'	'n/a'	'n/a'	'n/a'	'n/a'	'normal'
112	'n/a'	'n/a'	'n/a'	'n/a'	'n/a'	'normal'
113	'n/a'	'n/a'	'n/a'	'n/a'	'n/a'	'normal'
114	'n/a'	'n/a'	'n/a'	'n/a'	'n/a'	'normal'
115	'n/a'	'n/a'	'n/a'	'n/a'	'n/a'	'normal'
116	'redsmalldots'	'n/a'	'n/a'	'n/a'	'n/a'	'mild'
117	'n/a'	'n/a'	'n/a'	'n/a'	'n/a'	'normal'
118	'n/a'	'n/a'	'n/a'	'n/a'	'n/a'	'normal'
119	'n/a'	'n/a'	'n/a'	'n/a'	'n/a'	'normal'
120	'n/a'	'n/a'	'n/a'	'n/a'	'n/a'	'normal'
121	'n/a'	'n/a'	'n/a'	'n/a'	'n/a'	'normal'
122	'n/a'	'n/a'	'n/a'	'n/a'	'n/a'	'normal'
123	'n/a'	'n/a'	'n/a'	'n/a'	'n/a'	'normal'
124	'n/a'	'n/a'	'n/a'	'n/a'	'n/a'	'normal'
125	'n/a'	'n/a'	'n/a'	'n/a'	'n/a'	'normal'

126	'n/a'	'n/a'	'n/a'	'n/a'	'n/a'	'normal'
127	'n/a'	'hemorrhages'	'n/a'	'n/a'	'n/a'	'moderate'
128	'n/a'	'hemorrhages'	'n/a'	'n/a'	'n/a'	'moderate'
129	'redsmalldots'	'n/a'	'n/a'	'softexudates'	'neovascularisation'	'PDR'
130	'n/a'	'n/a'	'n/a'	'n/a'	'n/a'	'normal'